CR-183992

FINAL REPORT

NASA-CR-183992

June 19, 1989 - June 18, 1990

HYDROGEN INDUCED FRACTURE CHARACTERISTICS OF SINGLE CRYSTAL NICKEL-BASED SUPERALLOYS

June 18, 1990

Po-Shou Chen and Roy C. Wilcox

Department of Mechanical Engineering
Auburn University, AL 36849
(205) 844-3329

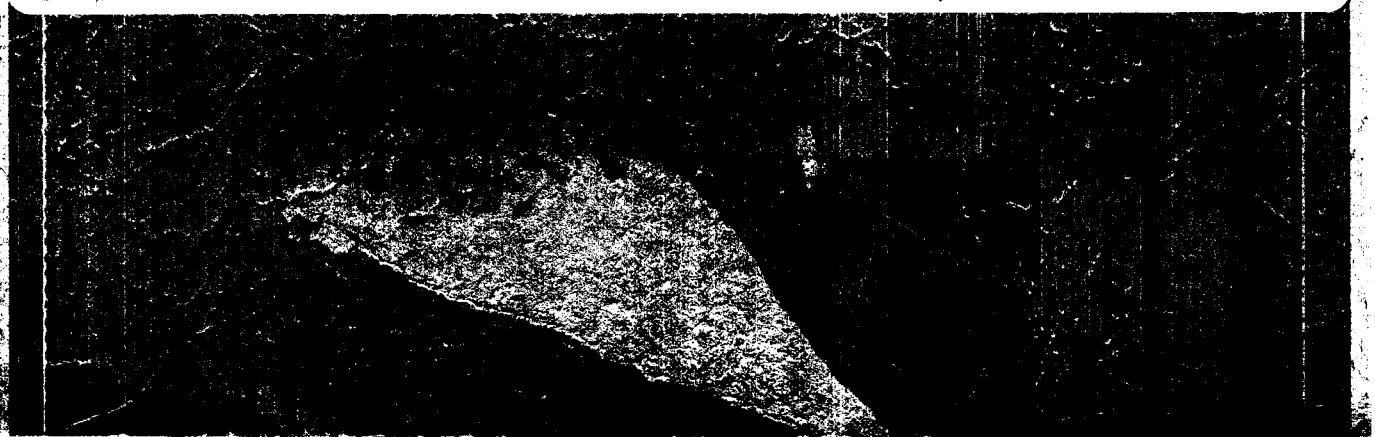

FINAL REPORT

NAS8-38184

June 19, 1989 - June 18, 1990

HYDROGEN INDUCED FRACTURE CHARACTERISTICS OF SINGLE CRYSTAL NICKEL-BASED SUPERALLOYS

June 18, 1990

Po-Shou Chen and Roy C. Wilcox

Department of Mechanical Engineering
Auburn University, Al 36849
(205) 844-3323

Prepared for
George C. Marshall Space Flight Center
Marshall Space Flight Center, Alabama 35812

TABLE OF CONTENTS

ABSTRACT

A stereoscopic method for use with X-Ray Energy Dispersive Spectroscopy of rough surfaces was adapted and applied to the fracture surfaces single crystals of PWA 1480E to permit rapid orientation determinations of small cleavage planes. The method uses a mathematical treatment of stereo pair photomicrographs to measure the angle between the electron beam and the surface normal. One reference crystal orientation corresponding to the electron beam direction (crystal growth direction) is required to perform this trace analysis. An area as small as 10 μm can be analyzed. The sensitivity of this technique was evaluated using a specimen with known orientation.

The microstructure of PWA 1480E was characterized before fracture analysis was performed. Gamma prime particles are orderly and closely aligned with edges along the [100], [010] and [001] directions. The cuboid morphology of the γ' precipitate was not influenced by the crystal growth orientation.

The fracture behavior of single crystals of the PWA 1480E nickel-based superalloy was studied. Notched single crystals with seven different crystal growth orientations near [100], [110], [111], [013], [112], [123], and [223] were tensile tested at room temperature in a helium atmosphere at 34 MPa. Specimens with a [110] orientation are strongest while those with a [100] orientation are the weakest. All specimens failed predominately by {111} type cleavage, which originated from combined slip on various {111} planes. TEM studies revealed that, in most cases, the deformation occurred inhomogeneously in intense slip bands lying on {111} planes. Both SEM and TEM studies indicated that {111} type slip was the controlling factor during cleavage fracture of single crystals of the PWA 1480E nickel-base superalloy.

The hydrogen-induced fracture behavior of single crystals of the PWA 1480E nickel-based superalloy was also studied. Notched single crystals with seven different crystal growth orientations near [100], [110], [111], [013], [112], [123], and [223] were tensile tested at room temperature in a hydrogen atmosphere at 34 MPa. The tensile strength degradation in hydrogen was anisotropic. Specimens with the [100] orientation had the greatest strength degradation while the crystal with the [111] orientation was the strongest. All specimens failed predominately by {100} type cleavage. By the conduction of TEM studies, hydrogen was found to enhance dislocation accumulation in the γ region. Microcracking along the {100} γ/γ' interfaces were observed in the area near the fractured surface. Both SEM and TEM studies indicated that {100} type cleavage was the controlling factor of hydrogen-induced cleavage fracture of single crystals of the PWA 1480E nickel-base superalloy at room temperature.

In order to understand the temperature dependence of hydrogen-induced embrittlement, notched single crystals with three different crystal growth orientations near [100], [110] and [111] were tensile tested at 871°C (1600°F) in both helium and hydrogen atmospheres at 34 MPa. Specimens tested in helium failed predominately by {111} type cleavage which originated from combined slip on various {111} planes. The specimen with the [100] orientation had the highest strength while the [110] was the weakest in helium. In hydrogen, all the specimens possessed very nearly the same tensile strength and failed predominately

by {111} type cleavage. Hydrogen effects appeared to be minimized at 871°C although strength degradation was still detected in the [100] and [111] crystals. In hydrogen, the [100] orientated specimen had the largest strength degradation while the [110] specimen showed a strength increase. A small amount of the (100) type cleavage was observed in the hydrogen-charged [100] specimen near the notch root. The presence of the (100) cleavage probably led to the largest strength degradation.

I. INTRODUCTION

One of the many applications for cast nickel-base superalloys is turbine blades for aircraft, space vehicles, and rocket engines [1,2]. Improvements in the mechanical properties of these alloys have been made through controlling composition and microstructure [3]. Also, single crystals of these alloys have been made to improve their high temperature mechanical properties [1,4]. The elimination of grain boundaries through the use of single crystals prevents segregation of elements such as carbon, zirconium and sulfur along grain boundaries. The elastic modules and other properties of single crystals are known to be anisotropic [1,5] but when properly orientated, single crystal structures have superior properties over conventional polycrystalline, equiaxial structures for applications such as turbine blades [1]. However, tests have shown that the use of hydrogen as a fuel rather than petroleum distillates may result in hydrogen environment embrittlement in nickel-base superalloys [1,2]. The strength degradation of single crystals in an hydrogen charged environment was found to be orientation dependent [1]. Little is known concerning this phenomenon, either as to the effects of crystal orientation or of phase orientation relationships. Therefore, the primary objectives of this work were to: (1) study the fracture behavior of PWA 1480E single crystals at 871°C in both helium and hydrogen; and (2) compare the fracture behavior of PWA 1480E in hydrogen with that of a hydrogen-free environment. Analytical electron microscopy and scanning electron microscopy were utilized in this investigation to study the microstructure and fracture behavior of the nickel-base superalloy single crystals.

II. HYDROGEN EMBRITTLEMENT IN NICKEL-BASED SUPERALLOYS

Hydrogen has a strong influence on both the mechanical and fracture behaviors of nickel-base superalloys [6-8]. Hydrogen can associate itself with dislocations in the nickel and influence the deformation behavior and enhance the hydrogen transport in the nickel lattice. Because hydrogen transport in nickel is slow, severe degradation from hydrogen charged into the bulk of these alloys is generally associated either with a hydrogen supersaturated lattice or involves dislocation enhanced hydrogen transport [8]. H. Vehoff and H. K. Klameth [9] reported that hydrogen induced embrittlement is a mixture of alternate slip on (111) planes and of local brittle fracture along (100) planes. The (111) planes were identified using the Y-shaped hillocks surface marking. They found that in a hydrogen environment, the materials could not bear the highly localized strains necessary for alternate slip, and thus it ruptured locally. No microcracks or voids were found in front of the crack tip.

An in-situ study of hydrogen effects on nickel was performed [10]. Fracture along the (111) type of planes was detected in both vacuum and in hydrogen. The crack advance mechanisms were observed to operate in hydrogen as well as in a vacuum. No hydride formation was detected. However, several significant differences between fracture in hydrogen and in a vacuum were observed. The principal one was that the stress required to induce crack advance was significantly reduced in the presence of hydrogen gas. Another significant difference was that the plastic zone formed in hydrogen at the front of the crack tip much narrower. Although fracture along (100) type planes was not detected,

embrittlement of nickel resulting from an hydrogen enhanced plastic process at the crack tip has been observed.

The effect of nickel on hydride formation in Ni-Cr-Fe alloys also has been reported [11]. Two types of hydrides were found: alpha hydride with a lattice constant ranging from 0.372 to 0.374 nm; and beta hydride with a lattice constant close to 0.362 nm. They found that surface grain boundary cracking existed in all the specimens but twin boundary cracking was detected only when the nickel content was over 60%. They also found that the amount of hydrogen absorbed in the form of a solid solution decreased and the amount of hydride increased with increasing nickel content. The hydride was quite unstable and easily decomposed at room temperature. The plastic deformation due to hydride formation was retained. Numerous dislocations were introduced by hydrogen charging and the mode of slip exhibited a more planar configuration compared to that arising from deformation without hydrogen charging.

E. L. Borowiecka [12] used X-ray diffraction techniques, microhardness and metallographic studies to detect hydrides in a nickel-base superalloy (HASTELLOY Alloy C-276) during cathodic charging at high hydrogen fugacities. The microhardness data strongly suggested that a hydride was formed although the location of the hydride reflections in the alloy did not correspond with those of NiH. The X-ray data indicated that an alloy hydride is formed with a lattice constant different from NiH. However, they were doubtful that hydride formation was responsible for embrittlement because the specimen which was the most susceptible to hydrogen embrittlement showed less surface damage. Therefore, they concluded that the existence of the hydride was

necessary, but not a sufficient condition, for the hydride mechanism of hydrogen embrittlement.

The mechanism of hydrogen embrittlement for polycrystalline nickel-base superalloys has been proposed [13]. Thermo-mechanical processing promoted the segregation of certain impurities to the grain boundary. At the grain boundary, the impurities interact with hydrogen and cause intergrangular failure at low applied stress. Impurity segregation at grain boundaries was determined to be the primary cause of hydrogen embrittlement.

Another report of hydrogen embrittlement in HASTELLOY Alloy C-276 (55%No, 16% Cr, 16 Mo, 5 Fe, 4W, 2 Co) also has been made by N. F. Fiore and J. A. Kargol [14]. They employed short-term and long-term aging to the materials before subsequent tensile testing in a hydrogen environment. They proposed that grain boundary segregation, which would accelerate intergrangular fracture alone, could not account for the observed mixed intergrangular-transgrangular fracture mode. They concluded that in either long-term or short-term embrittlement, planar slip and hydrogen transport by dislocations contributed to accelerated hydrogen stress cracking.

A more recent study of hydrogen effects in [001] oriented CMSX-2 nickel-base superalloy single crystals has been published by Baker et. al [10] and Dollar et. al [6]. C. L. Baker et. al found a hydrogen fugacity environment degraded the mechanical properties, when the kinetics of hydrogen transport were enhanced so that a significant volume of material was enriched with hydrogen. Surface voids acted to enhance the extent of hydrogen embrittlement by acting as strong

hydrogen trapping sites. The resulting high pressure within the void affected both crack initiation and growth, supplying both an additive stress component as well as a source of hydrogen to the crack tip region. The most important finding was that mode I fracture occurred in the embrittled region parallel to (001) planes, likely in association with preferential strain localization in the region of the γ/γ' interface. Fractographs of these alloys showed the associated fracture planes were parallel to the {100} type planes. This study also revealed that this {100} type fracture was most likely a result of hydrogen induced strain localization in the narrow ribbons of γ surrounding the cuboidal γ' particles. Outside the brittle region and completely within the uncharged samples, the fracture occurred along {111} slip planes by ductile shearing of the matrix.

M. Dollar and I. M. Bernstein [6] studied fracture in CMSX-2 nickel-base superalloy single crystals in the presence a of uniform high concentration of hydrogen and compared this to the hydrogen free situation. They found superdislocations were trapped in the γ matrix at the earliest stages of plastic deformation for both hydrogen free and hydrogen charged cases. In the absence of hydrogen, this accumulation appeared to be responsible for the high yield strength. Once yielding started, plastic flow was controlled by long ranged motion of unlocked superdislocations resulting in the observed low working hardening and very good ductility of the alloy. The most compelling hydrogen induced changes observed were enhanced dislocation accumulations in the γ matrix and extensive cross-slip of superdislocations. Both processes contributed to the increase in flow stress and the notable work

hardening that occurred prior to fracture. Hydrogen enhanced strain localization also occurred with dislocation intensification in the γ matrix, leading to premature cracking in the γ matrix. This was manifested macroscopically as failure parallel to the {100} faces of the γ' precipitates. TEM observations suggested that a difference existed in the macroscopic and microscopic nature of hydrogen-induced crack initiation and propagation. While microcracks macroscopically appeared to follow {100} planes, in reality they often occurred parallel to multiple {111} slip planes in the γ matrix.

Hydrogen embrittlement in single crystals of the nickel-base superalloy PWA 1480 has not been reported. However, two of the above studies [6,35] indicate that hydrogen was considered to reduce the {100} cleavage stress. Cleavage along {100} planes was the most fundamental mechanism of the hydrogen embrittlement of CMSX-2 single crystals. Due to the similar composition and microstructure between the CMSX-2 and the PWA 1480 alloys, some similar effects of hydrogen on PWA 1480 single crystals should be expected.

III. EXPERIMENTAL PROCEDURE

The PWA 1480E single crystals used in this study were furnished by NASA, Marshall Space Flight Center. The phases present in this alloy are primary γ and γ' [1]. Both phases have a face-centered cubic crystal structure with lattice constants very close to .3585 nm. A small amount of carbides and porosity also were found with the volume fraction of about 1.5% and 0.1% [1], respectively. The composition of the PWA 1480E alloy is proprietary but the nominal chemical composition of a PWA 1480 alloy is 5% cobalt, 10% chromium, 4% tungsten, 5% aluminum, 1.5% titanium, 12% tantalum with the balance nickel [2].

Notched single crystals of PWA 1480 with seven different crystal growth orientations were tensile tested by the Materials and Processes Laboratory at Marshall Space Flight Center. Single crystals were machined into tensile specimens, 8.5 mm in diameter, 50 mm long with a notch diameter of about 6 mm. The single crystal growth direction was the machined test direction. Tensile testing was performed at both room temperature and at 871°C in both helium and hydrogen atmosphere at the pressure of 34 MPa. Helium was considered to be a hydrogen-free atmosphere. Specimen growth orientations, test temperatures, and specimen numbers are given in Table 1.

A JEOL 840 SEM operating at 20 kv was utilized to study the fracture behavior. A stereoscopic method [15] was applied to permit rapid orientation determinations of small cleavage planes on a fracture surface. One reference crystal orientation corresponding to the electron beam direction was required to perform conventional trace analysis. A Microcomp Image Analysis System was utilized to study the

area fraction of secondary cleavage planes.

Table 1. PWA 1480E crystals.

Sample	Orientation	Specimen Number	Test Condition	
			Temperature (°C)	Environment
1	[100]	J279-2	22	He
2	[110]	H277-8	22	He
3	[111]	A278-8	22	He
4	[013]	B279-4	22	He
5	[112]	K280-8	22	He
6	[123]	B280-3	22	He
7	[223]	E277-4	22	He
8	[100]	J279-1	22	H_2
9	[110]	H277-7	22	H_2
10	[111]	A278-7	22	H_2
11	[013]	B279-2	22	H_2
12	[112]	K280-7	22	H_2
13	[123]	B280-1	22	H_2
14	[223]	E277-1	22	H_2
15	[100]	J279-3	871	H_2
16	[110]	J277-4	871	H_2
17	[111]	B278-3	871	H_2
18	[100]	J279-5	871	He
19	[110]	J277-5	871	He
20	[111]	B278-5	871	He

For TEM studies, thin foils were prepared. Electropolishing was conducted using an electrolyte [5] of 10% perchloric acid, 45% butylcellosolve ($C_6H_{12}O_6$), and 45% acetic acid at -1°C and 30 V for about 2 minutes. The TEM analyses were carried out on a JEOL 1200EX electron microscope at 120 kV. Conventional TEM techniques were used to investigate the microstructure, dislocation structure and slip systems involved. To determine the morphologies of the γ' precipitate in each

of the seven different crystal orientations, the precipitate was chemically extracted. Extraction was performed using an electrolyte containing 2 g of ammonium sulfate and 2 g of citric acid in 200 ml water [16]. The voltage was 4 to 5 volts for a extraction time of about 2 hours.

Quantitative area fraction measurements of {111} type cleavage plane were only performed for the cleavage planes with dimensions of larger than 10 μm. The remaining portion of the fracture surface consisted of very small non-{111} type cleavage planes. The small cleavage planes with dimensions of less than 10 μm were unable to be analyzed due to the limitation of the stereoscopic technique.

IV. RESULTS AND DISCUSSION

Fracture in Helium at 22°C

The PWA 1480E superalloy consists of about 40% of γ matrix and 60% of γ' precipitate. The cuboidal γ' precipitates are surrounded by the γ matrix network. In addition to γ and γ', the material also contained large particles of carbides (2 to 3% by volume) along with some voids and a small number of oxide inclusions.

In this study, PWA 1480E single crystals grown in seven different orientations, [100], [110], [111], [013], [112], [123], [223] were tensile tested in a helium atmosphere. The behavior in helium is considered to be the same as that in air. The tensile induced fracture and deformation behaviors were studied as a function of single crystal orientations. The cleavage plane orientations near and outside of the notch region are given in Table 2 for each of the seven crystals. The tensile strengths of the PWA 1480E single crystals as a function of the seven orientations are shown in Figure 1. These results are presented as a relative maximum tensile strength versus the [100] specimen. A specimen with the [110] orientation is stronger than any other orientation, while the [100] orientation is the weakest.

Conventional transmission electron microscopy and trace analysis were used to study dislocation structure and slip systems. A comparative analysis of the fracture orientations and deformation modes was made between the seven single crystal orientations [15]. Transmission electron microscopy studies were performed on single crystals of PWA 1480E to investigate the operative deformation mechanism which occurred during fracture. Thin foil specimens were cut very near

Table 2. Cleavage plane orientations near and outside of the notch area found in helium charged PWA 1480E single crystals [15].

CRYSTAL ORIENT.	NEAR NOTCH CLEAVAGE PLANE	ANGLE*	AREA % OF {111} CLEAVAGE PLANE	OUTSIDE OF NOTCH REGION CLEAVAGE PLANE	ANGLE*	RELATIVE TENSILE STRENGTH
[100]	{111}	54.7	18	{100} {111}	90 54.7	1.000
[110]	(111) (11$\bar{1}$)	35.3	16	{111} {$\bar{1}$11} {111}	90 90 35.5, 90	1.103
[111]	{111}	70.5	21	{011} {$\bar{2}$11} {111}	90 90 70.5	1.021
[013]	{111}	43.1, 68.6	29	{100} {0$\bar{3}$1} {111}	90 90 43.1, 68.6	1.032
[112]	{111}	19.5, 61.9 90.0	24	{1$\bar{1}$0} {02$\bar{1}$} {111}	90 90 19.5, 61.9, 90	1.065
[123]	{111}	22.2, 51.9 72.0, 90.0	25	{11$\bar{1}$} {2$\bar{1}$0} {111}	90 90 22.2, 51.9, 72.0, 90.0	1.090
[223]	{111}	11.4, 65.2 81.9	20	{1$\bar{1}$0} {21$\bar{2}$} {111}	90 90 11.4, 65.2, 81.9	1.055

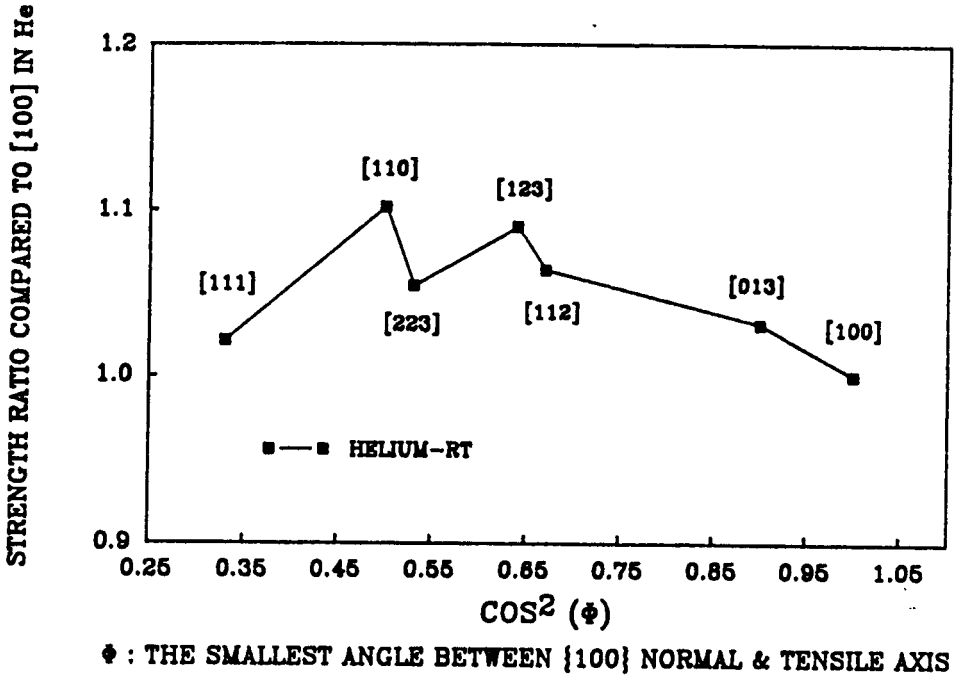

Figure 1. Relative tensile strength of PWA 1480E in helium as a function of seven different orientations.

the fracture surface with the foil normal perpendicular to the tensile axis. In most cases, the deformation was found to occur inhomogeneously in intense slip bands lying on {111} planes and aligned parallel to the different slip directions as shown in Figure 2. Dislocation accumulations within narrow γ regions and near the γ/γ' interface were detected (Figure 3). Furthermore, alternate cracks on {111} type planes along [011] and [01$\bar{1}$] directions were also observed (Figure 4). The TEM studies indicated that {111} type slip was the controlling factor during cleavage fracture of single crystals of the PWA 1480 nickel-base superalloy.

The deformation behavior of nickel-base single crystal superalloy has been studied [4,5,17]. In single crystal nickel-base superalloy Rene N4 [4], specimens with orientations near [100], [110], and [112], deformed in tension, all yielded by octahedral slip at room temperature. Single crystals with [112] orientations exhibited higher tensile strength than [100] and [110] crystals [5]. Different tensile behavior was observed in PWA 1480 single crystal nickel-base superalloy [18]. According to Shah et. al [18], the [100] orientation is stronger than the [110] orientation in tension at all testing temperatures between 0°C to 980°C. The experimental results found in this study were quite different compared to the two superalloys mentioned above. In PWA 1480 [18], all the possible models to explain tensile behavior including Schmid factor (the Schmid factor ratio for cube cross slip and the Schmid factor for the constriction stress) all failed to explain the tensile behavior.

In PWA 1480E, all the specimens failed primary by {111} type

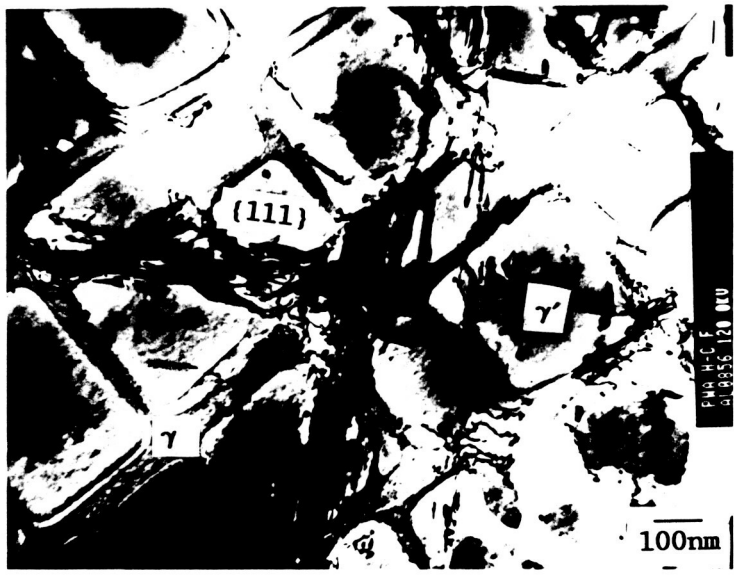

Figure 2. Bright field TEM micrograph with the foil normal parallel to the [100] stress axis showing intense bands lying on {111} planes

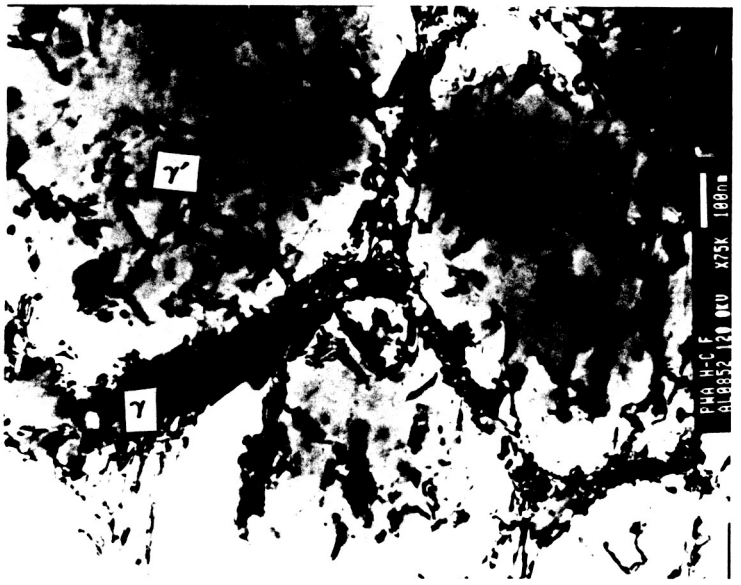

Figure 3. Deformation structure showing dislocation accumulation within the γ region and at the γ/γ' interface.

Figure 4. Cracking along <011> and <01$\bar{1}$> directions on a {111}slip plane.

cleavage regardless of the single crystal orientation. Although microscopic cube slip was detected by TEM, no obvious macroscopic {100} cube cleavage was observed on the fracture surface. Therefore, it is reasonable to assume that deformation took place and propagated primarily by octahedral slip. According to the TEM study, dislocations bypassing the γ' particles were not found near the fracture surface. To the contrary, dislocation accumulation around γ/γ' interfaces were observed in most of the areas. Therefore, the γ/γ' interface played an important role in the deformation and fracture behavior of single crystals of the PWA 1480E superalloy. Usually, intersecting dislocations in different glide planes produce work hardening. In this study, the work hardening effects seemed to be provided by both intersecting dislocations on different {111} slip planes and γ/γ' interfaces. Therefore, the number of slip systems available in each different specimen (Table 3) was used to interpret the different mechanical properties observed between different crystal orientations in the PWA 1480E superalloy.

As shown in Figure 1, the [110] specimen exhibited maximum tensile strength although only four slip systems were available (Table 3). In addition, during deformation, most of the dislocations tended to move and accumulate within the γ matrix. In other words, γ/γ' interface served as a strong barrier for dislocation motion. This indicated that plastic deformation was very inhomogeneous and localized around the γ/γ' interface. Therefore, the amount of dislocation accumulation around the γ/γ' interface should determine the strength of single crystals with different orientations. When dislocations on the available slip systems

Table 3. Summary of active slip systems and Schmid's factors for octahedral slip in each of the different specimens.

	Specimens Orientation and Schmid's Factor						
Slip systems	[100]	[110]	[111]	[013]	[112]	[123]	[223]
$(111)[0\bar{1}1]$	0	0.41	0	0.33	0.27	0.18	0.17
$(111)[\bar{1}10]$	0.41	0	0	0.16	0	0.18	0
$(111)[\bar{1}01]$	0.41	0.41	0	0.49	0.27	0.35	0.17
$(\bar{1}\bar{1}1)[011]$	0	0.41	0.27	0.33	0	0	0.12
$(\bar{1}\bar{1}1)[\bar{1}10]$	0.41	0	0	0	0	0	0
$(\bar{1}\bar{1}1)[101]$	0.41	0.41	0.27	0.25	0	0	0.12
$(\bar{1}11)[101]$	0.41	0	0.27	0.49	0.41	0.47	0.36
$(\bar{1}11)[110]$	0.41	0	0.27	0.16	0.27	0.35	0.29
$(\bar{1}11)[0\bar{1}1]$	0	0	0	0.33	0.14	0.12	0
$(1\bar{1}1)[\bar{1}01]$	0.41	0	0	0.25	0.14	0.12	0
$(1\bar{1}1)[110]$	0.41	0	0.27	0	0.27	0.18	0.29
$(1\bar{1}1)[011]$	0	0	0.27	0.33	0.41	0.29	0.37

entangled with the γ/γ' interface and became immobile, work hardening occurred. Thus, the rate of work hardening depended on the consumption rate of the mobile dislocations available. The greater the number of slip systems, the lower the tendency for work hardening.

The [110] specimen exhibited the highest tensile strength (Table 2) because only four slip systems were available and provided greater work hardening. The [100] specimen had the lowest strength because the eight available slip systems have identical Schmid factors (Table 3) and tend to slip easier compared to the other orientations. Another factor might be that most of the γ' particles grew with the cube edges aligned parallel to the [100], [010] and [001] directions of the γ matrix but not with the single crystal growth orientation. As shown in Table 2, (100) cleavage planes were detected in the [100] specimen. This was a good indication that the accumulation of dislocations along the (100) γ/γ' interface promoted the decohesion at the interface. Furthermore,

the (100) plane in a [100] specimen exhibits a greater resolved normal stress than the other orientations. The other six crystals have at least six available slip systems (Table 3). This would result in slower work hardening rates and lower strength compared to the [110] specimen (Table 2). These other six crystals would have a greater hardening rate and greater tensile strength than the [100] specimen which has eight possible slip systems.

In general, crystallographic cleavage does not occur in face-centered cubic (fcc) materials [19]. K. Aoki and O. Izumi [20] reported that the reasons that fcc materials do not fracture by cleavage are: (1) the dislocation pinning is so weak that the mobile dislocation density is always very high and the deformation is homogeneous; and (2) the dislocation velocity in fcc metals is independent of temperature and is always high except in high-strength alloys. For the PWA 1480E alloy, all seven different crystal orientation specimens failed predominantly by {111} type cleavage. This implies that this nickel-base superalloy is different from normal fcc materials. Coherent and order strengthening by γ' precipitates have been reported to play an important role during deformation [21]. Dislocations cutting through γ' particles will generate antiphase boundaries and make subsequent dislocation movement more difficult [21]. This explains why dislocation motion in nickel-base superalloy differs from that in usual fcc materials. This was confirmed by M. Dollar and I. M. Bernstein [6] who conducted a TEM study on the deformed No-base superalloy CMSX-2. At small strains most of the dislocations were trapped within narrow γ' regions and accumulated near γ/γ' interfaces. The accumulation of dislocation near

γ/γ' interfaces resulted in higher strength. Superdislocations cutting through both γ and γ' particles only occurred at higher strain levels. When the strain was high enough to move superdislocations through γ' particles, the subsequent plastic flow was controlled by long range movement of unlocked superdislocations. The present TEM study of the PWA 1480E alloy supports the view that dislocations have the tendency to accumulate near γ/γ' interfaces during deformation and slip along {111} planes as shown in Figure 3.

Cleavage type failure along {111} crystallographic planes in No-base superalloys also has been observed at room temperature [5,22,23]. Failure of single crystals of MAR-M200 always occurred along {111} crystallographic planes in an hydrogen-free atmosphere [6]. In single crystals of the nickel-base superalloy Rene N4, {111} cleavage planes and resulting fracture ridges were observed throughout the fracture surface [5]. In this investigation, a similar behavior was observed in PWA 1480E single crystals. Cleavage originated at the notch and propagated along crystallographic planes in all specimens. The observed cleavage planes were either a large single {111} plane or a combination of smaller {111} planes. As was observed, the single crystal orientation does not influence the initial cleavage plane orientation in the notch area except for the [110] specimen. In a [110] specimen, $(\bar{1}11)$ and $(1\bar{1}1)$ planes were not detected. This may be because the $(\bar{1}11)$ and $(1\bar{1}1)$ planes were perpendicular to the [110] tensile axis which resulted in a very small shear stress on these two planes. According to the Schmid equation [24] as shown in Table 3, the shear stress on the $(\bar{1}11)$ and $(1\bar{1}1)$ planes in the (110) specimen was equal to zero because

the tension axis was normal to the slip plane. This explains why $(\bar{1}11)$ and $(1\bar{1}1)$ planes were observed near the notch in all the specimens except the [110] crystal.

In addition, more than two {111} type planes were observed near the notch in all specimens with the exception of the [110] crystal. Thus slip was not confined to the planes with the maximum resolved shear stress. The presence of {111} type cleavage planes and fracture ridges outside the notch region should be the result of simultaneous slip or cross slip on {111} planes [25,26]. K. S. Chan et al. have reported that crystals of the Mar-M200 nickel-base superalloy had a tendency to slip along a single or a combination of {111} planes under multiaxial cyclic loads [27] or during compact-tension fatigue testing [24]. With few exceptions, they found that fracture planes were generally the planes of highest or second highest resolved shear stress. The exceptions occurred when fracture was occurring simultaneously by cracking on two cross-slip {111} planes, leading to the formation of ridges on the fracture surface. Coplanar slip relaxed the shear stress components of the crack-tip stress field, but had no effect on the normal stress components. The reason is that the coplanar slip did not provide displacements normal to the crack plane to relax the normal stress [27]. This explained why the {111} planes slipped alternately and formed ridges in all specimens although they did not show maximum resolved shear stress in all cases. The {111} cleavage planes slipped alternately from one to the other to provide rapid crack propagation [28] and normal stress relaxation [27].

The TEM observation of cracks formed on the {111} type planes

further supported the present SEM results that cleavage planes were either a single large {111} plane or a combination of smaller {111} planes. Therefore, what appeared to be brittle cleavage along crystallographic planes at the notch root did in fact involve plastic deformation because most of the cleavage occurred on the {111} planes. During the deformation process, both γ and γ' slipped on {111} planes. Thus, both SEM and TEM observations indicate that {111} type slip was the controlling factor of fracture in the PWA 1480E single crystals.

The combined SEM and TEM results of this study suggest the following {111} type cleavage mechanism in helium. At the early stage of testing, {111} type slip occurred very quickly. Soon, dislocations were trapped within the narrow γ matrix region and gradually accumulated around γ/γ' interfaces. This accumulation of dislocations would hinder subsequent superdislocation movement. As loading continued, more intensive planar slip on {111} planes was produced and cut through both γ and γ' particles. Once the movements of single {111} slip dislocation were interrupted, cross slip from one {111} to another {111} plane occurred to keep the dislocations moving. After considerable slip, dislocation entanglements made the movement of dislocations on {111} planes very difficult and resulted in cleavage on {111} crystallographic planes. Simultaneous cracking on two or more cross-slip {111} planes occurred to relieve normal stresses and promoted the main crack propagation. As the tensile test continued, new mobile dislocations along {111} planes were generated in the undeformed area. These dislocations were not available for continuing pre-existing {111} slip because most of the dislocations became sessile near the notch region.

When the number of mobile dislocations became too small to provide alternate slip, fracture occurred locally. The formation of {111} cleavage at the notch root was due to the rapid decrease in the mobile dislocation density resulting from dislocation entanglement. Slip planes of the {111} type located outside the notch region formed before final fracture occurred. The non-{111} types of cleavage planes observed in all crystals did not play an important role but were the result of final rupture after the formation of {111} type cleavage.

The following summaries resulted from the investigation of helium-charged tensile induced fracture in single crystals of the nickel-based superalloy PWA 1480E:

1. γ' particles are orderly and closely aligned with edges along the [100], [010] and [001] directions. Different crystal growth orientations did not affect the morphology of γ' particles.
2. Dislocation accumulation around γ/γ' interface forming strong barriers for subsequent dislocation movement is the primary strengthening mechanism at room temperature.
3. The availability and activity of slip systems played an important part to the strength variation between different orientations.
4. Tensile induced {111} cleavage in helium originated from combined slip on {111} planes.
5. The occurrence of {111} type of cleavage were qualitatively independent of the single crystal orientations.
6. The occurrence of {111} cleavage planes outside the notch area

was not related to the testing atmosphere.

7. Cracking along γ/γ' interface was not observed in all the specimens with seven different crystal growth orientations.

Fracture in Hydrogen at 22°C

The primary objectives of this work were to: (1) characterize the fracture surface of hydrogen charged single crystals of PWA 1480E as a function of crystal orientation; (2) study the deformation and fracture behavior as a function of crystal orientation, and (3) compare the fracture behavior in hydrogen with that of a hydrogen-free environment.

In order to determine the role of hydrogen, fracture surfaces of notched tensile specimens of single crystals of PWA 1480E with seven different crystal growth directions, [100], [110], [111], [013], [112], [123], [223], were examined. A comparative analysis of the fracture behavior was made between these crystals to determine the degree of hydrogen embrittlement as a function of crystal orientation. In addition, the deformation mode and crystallographic cleavage fracture were compared between specimens charged in hydrogen and in a hydrogen-free atmosphere to better understand the hydrogen embrittlement phenomenon. Analytical electron microscopy and scanning electron microscopy were utilized in this investigation to study the hydrogen-induced fracture of PWA 1480E single crystals.

The relative tensile strengths of the seven crystals are given in Table 4 and plotted in Figure 5. These results are presented as relative tensile strength normalized to the [100] specimen. The [111] crystal was stronger than any other orientation, while the [100] crystal

Table 4. The cleavage planes orientations near and outside the notch area found in hydrogen charged single crystals of the No-base superalloy PWA 1480E [15].

CRYSTAL ORIENT.	NEAR NOTCH CLEAVAGE PLANE	ANGLE	AREA % OF {111} CLEAVAGE PLANE	OUTSIDE OF NOTCH REGION CLEAVAGE PLANE	ANGLE*	RELATIVE TENSILE STRENGTH to [100] He
[100]	(100)	0	8%	{100} {111}	90 54.7	0.57
[110]	(100),(010)	45.0	8%	$(1\bar{1}1),(\bar{1}11)$ {111}	90 35.3,90.0	0.87
[111]	(100),(010) (001)	54.7	8%	(0110, (211) {111}	90 70.5	0.90
[013]	(001)	18.4	8%	(100), $(0\bar{3}1)$ {111}	90 43.1,68.6	0.67
[112]	(001)	35.3	9%	$(1\bar{1}0)$, $(02\bar{1})$ {111}	90 19.5, 61.9 90	0.78
[123]	(001)	36.7	10%	(111), (210) {111}	90 22.2, 51.9 72.0, 90.0	0.80
[223]	(001)	43.3	10%	(110), (212) {111}	90 11.4, 65.2 81.9	0.80

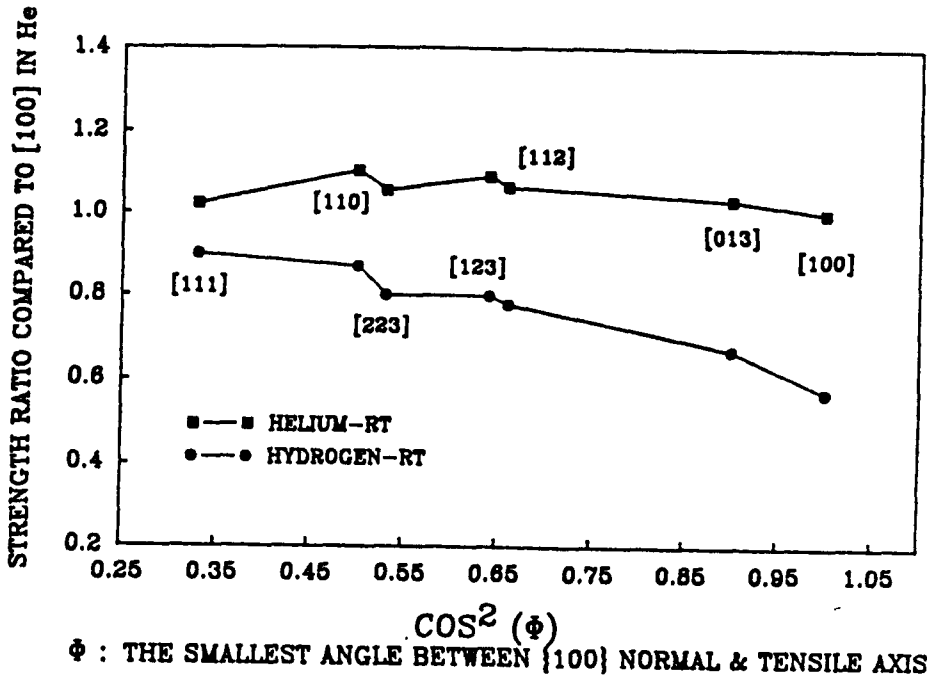

Figure 5. Relative tensile strength of PWA 1480E as a function of seven different different orientations. All strengths normalized to [100] crystal in helium at 22°C.

was the weakest.

In order to further study the hydrogen-induced cleavage behavior, TEM studies were carried out on fractured specimens to investigate the microscopic fracture mechanisms. Thin foil specimens (near the fracture surface) were cut with the normal perpendicular to the tensile axis. Deformation was found to occur inhomogeneously in intense slip bands lying on {111} planes and aligned parallel to the different slip directions as was observed in helium charged specimens. Dislocation accumulation within the narrow γ region and cracks along the alternate [011] and [01$\bar{1}$] directions on the {111} type planes were observed (Figure 6).

Superdislocations with "V" shaped configuration were found in the γ' particles (Figure 7). This is a typical morphology of {100} type superdislocations [29]. In addition to [110] and [011] cracking on the {111} planes, microcracking along {111} slip planes within the γ matrix (Figure 8a) or along {100} γ/γ' interfaces was detected (Figure 8b). This revealed that, in addition to the cracking cutting across both γ and γ' particles, cracking could occur in the narrow γ region on {111} planes or be deflected by γ' particles leading to interfacial cracking on {100} planes. In a previous study [4], the dislocation structure in helium charged specimens was similar to that found in the hydrogen charged specimens in this work. The primary differences were the formation of {100} type slip and cracking along the γ/γ' interface in an hydrogen atmosphere.

Examination of all the hydrogen charged specimens revealed that fracture occurred predominantly along {100} type planes near the notch

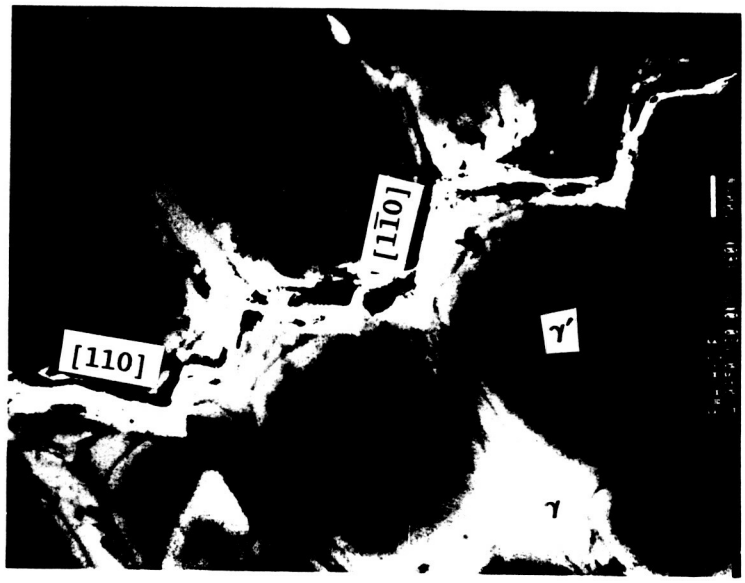

Figure 6. Cracking along the [110] and [01$\bar{1}$] directions on a {111} slip plane.

Figure 7. "V" shaped superdislocation.

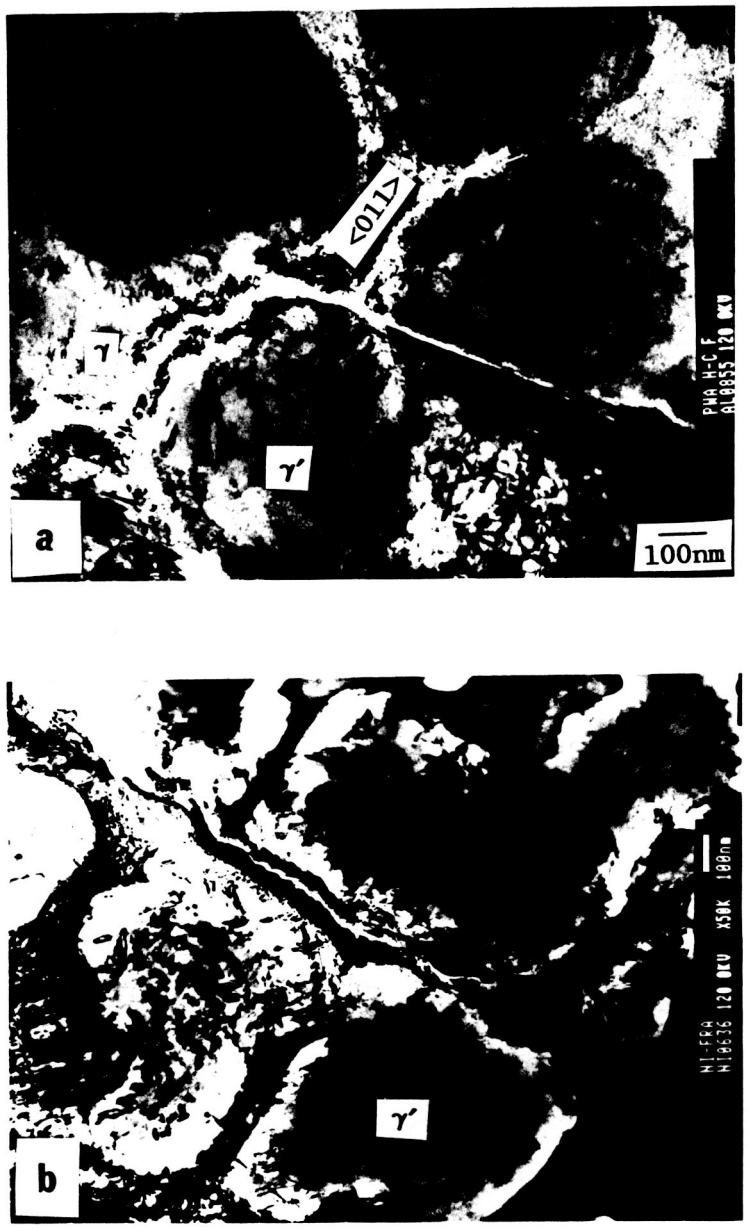

Figure 8. (a) Cracking along the [011] direction was locally deflected by γ' and advanced along the γ/γ' interface. (b) Cracking within the γ region with propagation along {111} planes.

region. The occurrence of {100} cleavage planes appeared to be independent of the single crystal orientation. The TEM work showed that {100} type cleavage planes were associated with γ/γ' interfacial cracking. Therefore, the {100} type cleavage along the γ/γ' interfaces was very likely a result of hydrogen induced strain localization within the γ network. A similar phenomenon was observed in the CMSX-2 with a single crystal orientation of [001] [7]. M. Dollar and I. M. Bernstein [6] studied the dependence of dislocation structure on the amount of strain generated by conducting tensile tests on CMSX-2 single crystals with orientations near [001]. They found that most of the dislocations were trapped in the γ near the γ/γ' interface region in the early stage of deformation because superdislocations were not able to travel far through the interface. The accumulation of dislocations within the γ increased the local hydrogen concentration due to dislocation trapping. This trapping of hydrogen then enhanced dislocation generation in the vicinity of the γ/γ' interface. These accumulated dislocations then formed barriers for subsequent superdislocation movement across the interface. To reduce the antiphase boundary (APB) energy in a hydrogen-free atmosphere, a superdislocation had the tendency to cross slip from {111} to {100} planes when stressed at high temperature [6,17,30]. This was because the APB energy was lowest on the {100} planes. In this study, superdislocations with a "V" shaped configuration were found in γ' particles (Figure 7). This was a typical morphology of {100} type superdislocations [29]. Hydrogen, thus, enhanced superdislocation cross-slip from {111} to {100} planes in the PWA 1480E alloy. Cracking within γ and along the γ/γ' interface were detected as shown in Figure

8. The microscopic interfacial cracking further supported the TEM results that cracks which occurred along γ/γ' interfaces were not necessarily composed of short segments of multiple {111} slip planes.

Tensile tests on hydrogen charged nickel-base superalloys tended to be affected by hydrogen transport [8]. The extent of embrittlement was closely related to the extent of subsurface hydrogen penetration either through the lattice, along interfaces, or associated with mobile dislocations [31]. Hydrogen transport by dislocations can be enhanced by tensile testing if the strain rate is not too high. In this study, the {100} type cleavage region (notch region) only extended about 8000 nm away from the notch. This was an indication that hydrogen did not penetrate very deeply into the specimens during tensile testing.

With only about 8 to 10% of the fracture surface in each specimen, and then only outside of the notch area, being {111} type cleavage, interfacial cracking between γ and γ' on {100} planes was likely a result of hydrogen induced embrittlement in PWA 1480E single crystals. The strain which concentrated locally in the γ/γ' interface, could accelerate crack extension along the interface, leading to a greater ductility loss. The formation of {111} type cleavage can be explained by the same mechanism which was applied to helium charged specimens [4]. The presence of {111} type cleavage planes and fracture ridges outside the notch region should be the result of simultaneous slip or cross slip of {111} planes. The formation of {111} cleavage planes was not a result of hydrogen induced fracture in single crystals of PWA 1480E. Nickel hydride was not detected in any of the specimens although hydrides have been detected in some hydrogen charged No-base alloys

[11,12]. According to Hinotani et al. [11], hydrides were very unstable and decomposed very rapidly. The primary effect of hydrides was the formation of hydride induced cracks along grain boundaries at the interface of {111} planes during the decomposition of hydrides. Lunarska-Borowiecka et al. [12] also observed similar features. They detected nickel hydride in a nickel-base superalloy and found cracking after hydrogen charging. They indicated that hydrides do form and result in surface cracking after hydride decomposition. Because the alloy which was most susceptible to hydrogen embrittlement showed less surface damage, they concluded that the existence of the hydride was only a necessary but not a sufficient condition for the hydride formation mechanism of hydrogen embrittlement. More recent studies have shown that hydrides in nickel-based systems could be produced only by extremely severe cathodic charging [7]. Pielaszek [32] reported that the pressure of nickel hydride formation at ambient temperature was 0.6 GPa, whereas the decomposition pressure was about 0.34 GPa. In the present study, hydride formation was not expected because all specimens were charged by gaseous hydrogen at room temperature at a pressure of 34 MPa which is much smaller than 0.6 GPa. In addition, no observable surface cracking, which was a typical feature of hydride formation and decomposition, was found in longitudinal section of the specimens. This finding further supports the hypothesis that hydrides were not present in the specimens during tensile testing.

In addition, no subsurface voids were found to be associated with {100} cleavage near the notch although subsurface voids were reported to enhance the extent of hydrogen embrittlement [7]. Therefore, the

present observations demonstrate that hydrogen induced fracture was a result of cleavage fracture primary along γ/γ' interface parallel to {111} planes. A possible mechanism of hydrogen induced fracture can be proposed as follows.

Both SEM and TEM observations revealed that {100} cleavage was the main controlling factor of hydrogen embrittlement in single crystals of PWA 1480E nickel-base superalloy. At the early stage of tensile testing, {111} slipping may occur and soon dislocations become trapped in the γ region. Tensile testing produced planar slip which enhanced dislocation transport and led to high local concentrations of hydrogen in the γ region. The high concentration of hydrogen resulted in severe dislocation pinning and subsequently dislocation accumulation along γ/γ' interfaces and the γ matrix. The accumulation of dislocations hindered subsequent superdislocation movement. At room temperature, even though the dislocation motion on {111} planes became very difficult, slip on {100} systems could not be activated because the frictional stress on {100} planes was generally high at low temperature [6]. Therefore, the presence of hydrogen could enhance the cross-slip of superdislocation from {111} to {100} planes when work hardening caused the dislocation motion on {111} planes to become extremely difficult. Both enhanced cross-slip of superdislocations and enhanced dislocation accumulation in the γ region would hinder subsequent superdislocation movement and increase the rate of working hardening. When dislocations accumulated too much in the γ to provide a free path for dislocation movement, then straight interfacial cracking occurred (Figure 8). When the free path in the γ region was decreased by accumulated dislocations but was still

available, short segment slipping on {111} planes inside the γ region occurred. Both cases result in {100} type of interfacial cracking along the γ/γ' interface as seen in Figures 8.

As the tensile test continued, new mobile dislocations along {111} planes were generated in the undeformed area but they were not available for pre-existing {111} slip because most of the dislocations became sessile near the notch region. When mobile dislocations became exhausted, fracture was accelerated. Therefore, the formation of {100} cleavage should be a result of rapid decrease in the mobile dislocation density resulting from dislocation pinning due to cube cross-slipping and dislocation entanglement inside the γ region. Slip on {111} planes occurred before final fracture occurred. The other types of cleavage planes, except {100} and {111} observed in all the specimens could not be related to the hydrogen induced embrittlement but were the result of final rupture after the formation of {111} and {100} cleavage.

As shown in Table 4, the specimen with the [100] orientation had the lowest strength while the [111] crystal was the strongest. Moreover, the strength degradation of single crystals in a hydrogen charged environment compared to a hydrogen-free environment [4] was found to be orientation dependent. The amount of tensile strength degradation (%) of PWA 1480E tested in hydrogen as a function of single crystal orientation is given in Figure 9. As shown, the specimen with the [100] orientation had the highest strength degradation while the [111] crystal degraded the least. The single crystal growth orientation had no or very little influence on the microstructure of the PWA 1480E No-base superalloy [25]. Therefore, the anisotropy degradation of

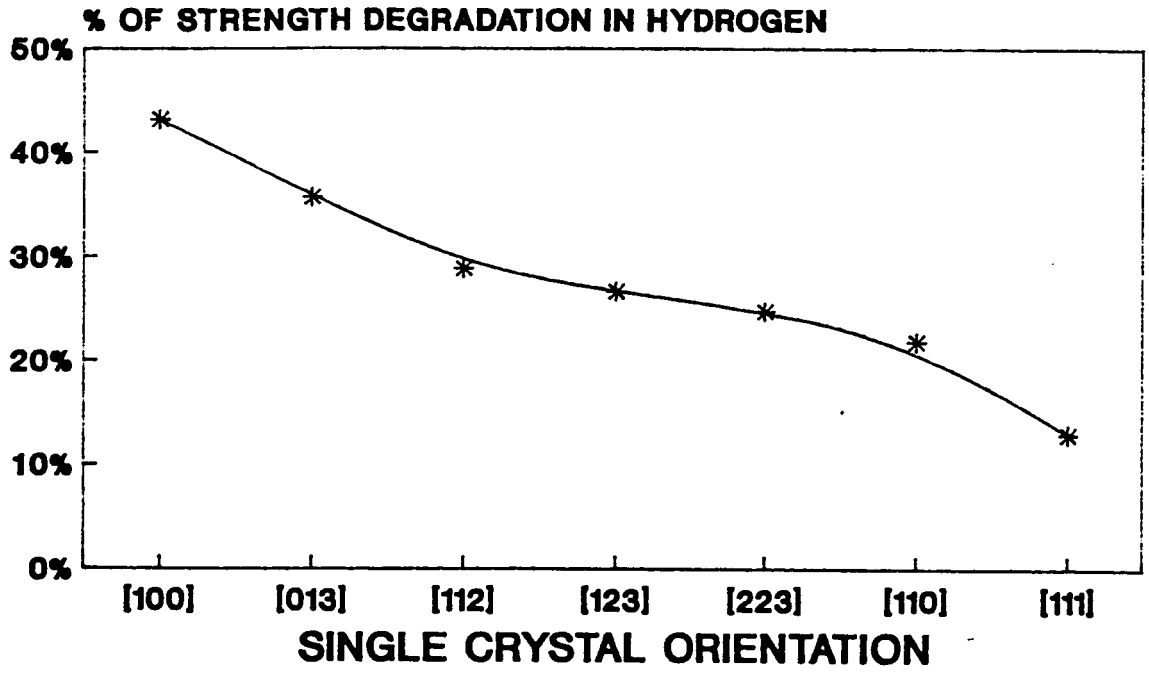

Figure 9. Tensile strength degradation in hydrogen of PWA 1480E as a function of the seven different orientations.

strength should have some relationship to hydrogen induced cleavage behavior. As shown in Table 4, cleavage fracture occurred on {100} type planes near the notch root in hydrogen charged single crystals and was independent of the single crystal orientation. Thus, some relationship must exist between the cleavage plane orientation and anisotropic degradation. All possible angles between {100} planes and the various single crystal orientations are given in Table 5.

Table 5. Angles between the normal of {100} planes and the single crystal orientation.

Plane	Single Crystal Orientation						
	100	110	111	013	112	123	223
(100)	0°	45°	54.7°	90°	65.9°	74.5°	67.7°
(010)	90°	45°	54.7°	71.6°	65.9°	57.7°	67.7°
(001)	90°	45°	54.7°	18.4°	35.3°	36.7°	43.3°

Careful examination of Tables 4 and 5, revealed that hydrogen induced cleavage always occurred along one of the {100} planes which had the smallest angle between the normal to the {100} type plane and the tensile axis. In addition, the amount of degradation increased with decreasing angle between the normal to the {100} plane and the tensile (crystal) axis. Therefore, hydrogen-induced brittle fracture of PWA 1480E single crystals was considered in relation to the angle between the normal to the {100} type plane and the tensile axis. The plot of the cosine square of this angle ($\cos^2 \phi$) vs the single crystal

orientation is shown in Figure 10.

If the anisotropic degradation of strength was primarily controlled by the normal stress on the {100} plane, the amount of strength degradation should decrease with decreasing the angle ø as shown by the relationship

$$\sigma = P/A\ (\cos^2\phi).$$

The larger the angle ø, the lower the normal stress required to induce crack propagation on the {100} plane. The combined plot of Figure 9 and 10 is given in Figure 11. As shown in Figure 11, the amount of strength degradation had good agreement with the normal stress on {100} cleavage planes. This orientation dependence suggested that hydrogen-induced fracture occurred by cleavage on the {100} plane with the smallest angle between the normal to the {100} planes and the crystal axis. The fracture stress increased with increasing the angle ø and fracture then occurred when the resolved normal stress to the {100} planes attained a critical value. In other words, the greatest degradation occurred in the [100] specimen because of the least applied fracture stress required to induce cleavage on the (100) plane. The microscopic observation of mismatch, misorientation, volume fraction and morphology of γ', revealed no deviation between single crystal growth orientation [15]. Therefore, it can be concluded that cleavage fracture of the hydrogen charged nickel-base superalloy was mainly governed by {100} cleavage. The controlling factor of anisotropic strength degradation was the angle between the normal to the {100} planes and the tensile axis. In the specimen with the [100] orientation, the normal to the (100) plane was 0° to the tensile axis and this resulted in the

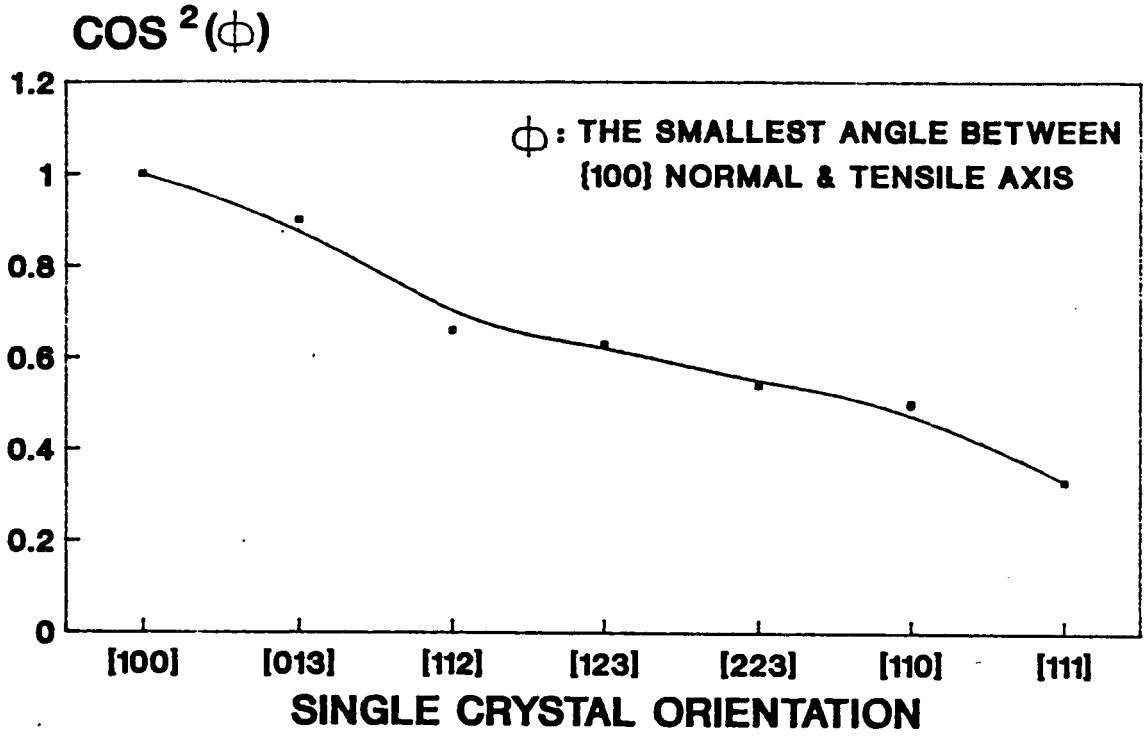

Figure 10. The relative resolved normal stress which existed to induce {100} type cleavage as a function of single crystal orientation.

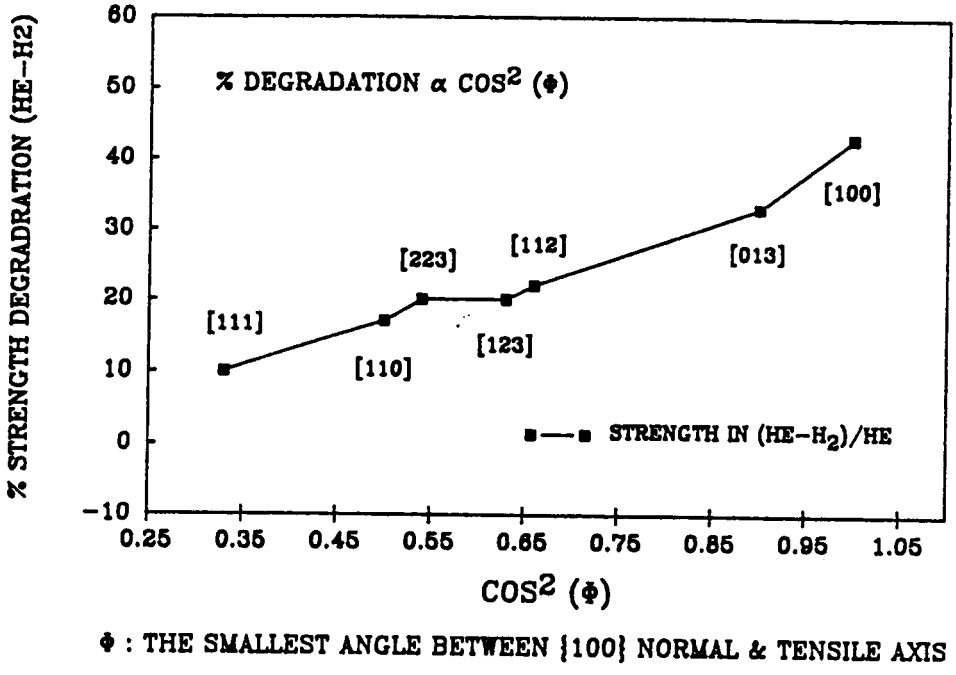

Figure 11. Tensile strength degradation in hydrogen of PWA 1480E as a function of the relative resolved normal stress existing to induce {100} type cleavage.

largest strength degradation. On the contrary, the [111] specimen had the highest resistance to hydrogen charging due to a high angle of about 57° between the normal to the (100) cleavage plane and the tensile axis. Therefore, the anisotropic degradation of strength in hydrogen charged PWA 1480E single crystals could be explained as a function of the smallest possible angle between the crystal (tensile) axis and the normal to the {100} planes.

The following summaries resulted from the investigation of hydrogen induced fracture in notched single crystals of the nickel-based superalloy PWA 1480E:

1. Hydrogen enhanced cleavage along {100} planes was the most important mechanism of hydrogen-induced embrittlement in single crystals of the nickel-base superalloy PWA 1480E.
2. {111} cleavage was only observed outside the notch region. {100} cleavage was the primary feature of hydrogen charged specimens.
3. {100} type cleavage in hydrogen was associated with either cracking along the γ/γ' interfaces or along {111} planes in the γ matrix.
4. The occurrence of {100} and {111} types of cleavage were qualitatively independent of the single crystal orientations.
5. The angle between the normal to the {100} planes and the crystal orientation had a strong affect on the strength degradation.

6. Outside of the notch region, the fracture surface of specimens tested in hydrogen appeared very similar to those tested in helium. Differences in the fracture surfaces were located primarily near the notch region.
7. The occurrence of {111} cleavage planes outside the notch area was not related to the testing atmosphere.
8. The absence of {100} type planes in the helium charged specimens supported that {100} cleavage was induced by hydrogen.

Fracture at 871°C

The deformation behavior of single crystals of nickel-based superalloys has been studied [1,4,5,18,19,33]. PWA 1480 was found to have an increase in strength with increasing testing temperature [18]. This unusual behavior was due to a thermal activated cube cross-slip process inhibiting dislocation glide. Similar cube cross-slip was found in single crystals of the alloy Rene N4 [5]. In Rene N4, specimens with [100] and [110] orientations exhibited octahedral slip at room temperature, and at 760 and 980°C. However, primary cube slip occurred for the [112] oriented specimen at 760 and 980°C.

Nickel-base superalloys have been shown to be susceptible to hydrogen embrittlement [1,6,7,33]. Moreover, the strength degradation of single crystals in a hydrogen environment was found to be orientation dependent at room temperature [1,33]. Hydrogen-induced cleavage along the γ/γ' interface was found in a [001] oriented CMSX-2 single crystal [6,7,33]. However, hydrogen effects at high temperature (871°C) on

single crystals of nickel-base superalloys have not been reported. In order to determine the role of hydrogen, fracture surfaces of notched tensile specimens of single crystals of PWA 1480E with three different crystal growth directions, [100], [110], [111] were examined. A comparative analysis of the fracture behavior was made between the crystals with three different orientations to understand the susceptibility of hydrogen embrittlement under a variety of single crystal orientations. In addition, the deformation mode and the crystallographic cleavage fracture were compared between specimens charged in hydrogen and in a hydrogen-free atmosphere. Such a comparative analysis was necessary for a better understanding of the hydrogen embrittlement phenomenon at high temperature.

In this work, the study of the tensile fracture behavior of single crystals of the superalloy PWA 1480E at 871°C was performed by the use of SEM fractography. The tensile induced fracture and deformation behaviors were studied as a function of single crystal orientations. Macroscopic traces of cube slip were not found in all specimens. The differences in strength as affected by crystal orientations and test temperature will be discussed in terms of Schmid's factor, availability of slip systems, and the γ/γ' interface. A stereoscopic technique [15] combined with the use of planar γ' morphologies were applied to identify the cleavage plane orientation.

The tensile strengths of PWA 1480E single crystals tested in helium as a function of three different orientations are given in Table 6. These results are presented as the relative maximum tensile strength versus the [100] specimen. In helium, the specimen with the [100]

orientation was the strongest while the [110] crystal was the weakest. The relative tensile strengths versus the [100] specimen in hydrogen as a function of the three orientations are given in Table 7 and plotted in Figure 12. In hydrogen, the [111] orientation specimen was stronger than any other orientation, while [110] orientation was the weakest.

To better understand the relationship between the orientation and the environmental dependence of the tensile strength, specimens with various orientations were studied using SEM fractography. Carbides were found in all fracture surfaces. However, no evidence was found to indicate that fracture in any crystal was related to the carbides. Quantitative area fraction measurements of the {111} type cleavage plane were only performed for the cleavage planes with dimensions of larger than 10 μm. Cleavage areas with dimensions less than 10 μm were not analyzed because of the limitation of the stereoscopic technique.

A. Fracture in Helium at 871°C

1. [100] Specimen

The top and side view fractographs of the [100] orientated crystal are shown in Figure 13. Close observation in the region of the notch root at higher magnification (Figure 14a) revealed a jagged appearance which seemed to be the result of cleavage along specific crystallographic planes. Stereoscopic measurements of the normals to the cleavage planes near the notch gave an angle of about 55° with respect to the [100] crystal axis. Cleavage planes with this angular relationship were then determined by trace analysis to be {111} type planes. An equilateral triangular type network further confirmed the

Table 6. Cleavage plane orientations near the notch area and the area fraction of {111} plane found in helium charged PWA 1480 single crystals at 871°C.

CRYSTAL ORIENT.	NEAR NOTCH CLEAVAGE PLANE	ANGLE*	AREA % OF {111} CLEAVAGE PLANE	RELATIVE STRENGTH VS. [100] in He @ 22°C %
[100]	{111}	54.7	54%	0.94
[110]	(111) (11$\bar{1}$)	35.3	58%	0.76
[111]	{111}	70.5	60%	0.87

* Angle between the cleavage plane normal and the crystal axis.

Table 7 Cleavage plane orientations near the notch area and the area fraction of {111} plane found in hydrogen charged PWA 1480 single crystals at 871°C.

CRYSTAL ORIENT.	NEAR NOTCH CLEAVAGE PLANE	ANGLE*	AREA % OF {111} CLEAVAGE PLANE	RELATIVE STRENGTH VS. [100] in He @ 22°C %
[100]	{111} (100)	54.7	42	0.85
[110]	(111) (11$\bar{1}$)	35.3	45	0.82
[111]	{111}	70.5	38	0.85

* Angle between the cleavage plane normal and the crystal axis.

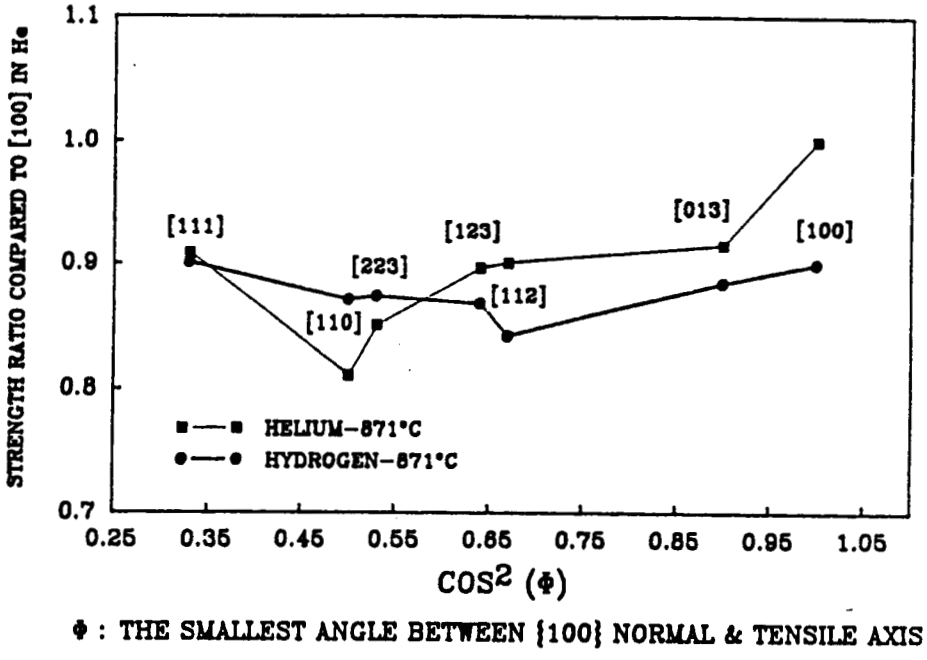

Figure 12. The relative tensile strength of PWA 1480E at 871°C as a function of orientations and testing atmosphere. These results are presented as a relative maximum tensile strength versus the [100] helium-changed specimen.

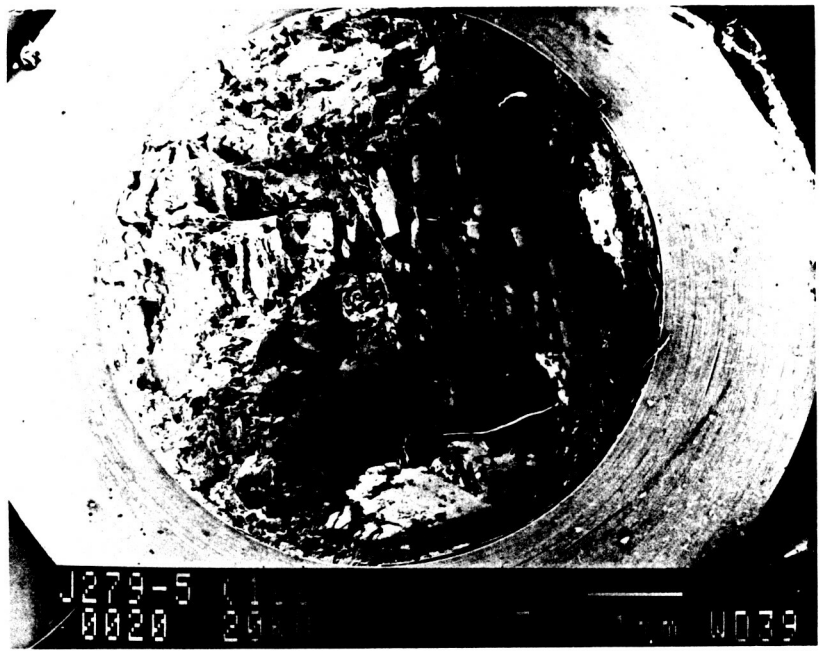

(a)

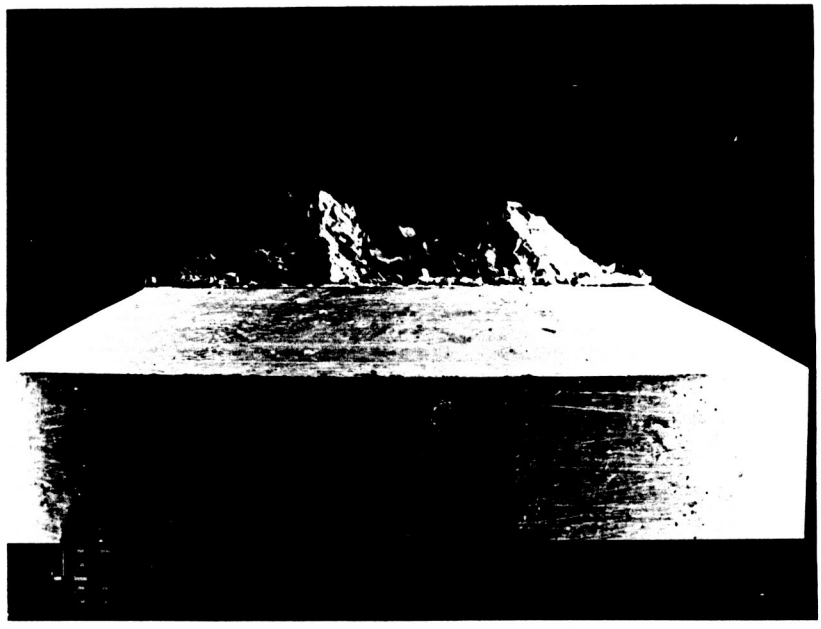

(b)

Figure 13. SEM fractograph of the [100] specimen tested in helium at 871°C: (a) top view. (b) side view.

(a)

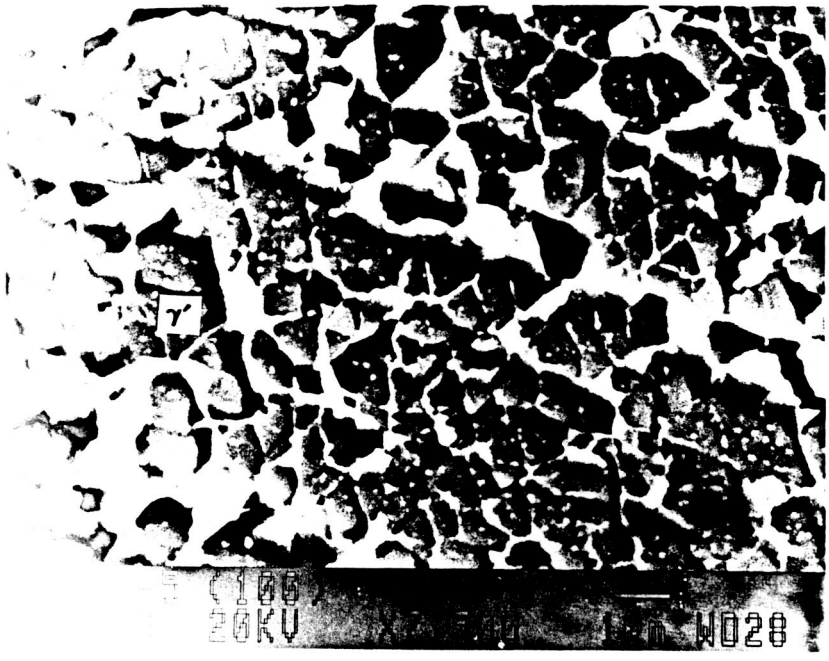

(b)

Figure 14. (a) {111} type of cleavage planes found in the [100] specimen showing the notch area. (b) Fractograph taken at high magnification showing the triangular network.

determination (Figure 14b). Such a microstructural network was typical of cleavage fracture on the {111} type planes in γ'. Cleavage on {111} planes was not confined to the notch area. Outside of the notch region toward the specimen center, {111} cleavage planes were also found.

The overall area fraction of {111} type cleavage planes was determined by image analysis to be about 54% of the entire fracture surface. Therefore, the fracture behavior of the [100] specimen tested in helium could be summarized as fracture mainly on the {111} planes in the notch region followed by {111} type cleavage outside of the notch area. The cleavage plane orientations near the notch and the overall area fraction of {111} cleavage planes are given in Table 6.

2. [110] Specimen

The top and side view fractographs of the [110] specimen are shown in Figure 15. Close examination of the fracture surface revealed several crystallographic cleavage planes. Stereoscopic measurements gave an angle of 35° between the cleavage plane normals and the [110] crystal axis. These cleavage planes were then determined either to be (111) or $(11\bar{1})$ planes (Figure 16a). The identification of the {111} type cleavage plane was confirmed by the appearance of the equilateral triangular type of network (Figure 16b). In addition to the (111) and $(11\bar{1})$ planes found near the notch, {111} type cleavage planes were also detected outside the notch region toward the specimen center.

The area fraction of the (111) and $(11\bar{1})$ cleavage planes were determined by image analysis to be close to 58%. Approximately 50% of the {111} type cleavage planes were located near the notch area. Therefore, the fracture behavior of the [110] specimen tested in helium

could be summarized as fracture mainly on the (111) and (11$\bar{1}$) type planes in the notch region followed by {111} type cleavage outside the notch area. The cleavage plane orientations near the notch and the overall area fraction of {111} cleavage planes are given in Table 6.

3. [111] Specimen

The top and side view fractographs of the [111] specimen are shown in Figure 17. Closer examination of the fracture surface revealed several crystallographic cleavage planes. Stereoscopic measurements gave an angle of about 70° between the cleavage plane normal and the [111] crystal axis. These cleavage planes were then determined to be of the {111} type planes (Figure 18a) and were further confirmed by the triangular type γ' network (Figure 18b). Therefore, the (111) specimen failed primarily by {111} type cleavage near the notch. Cleavage planes of the {111} type also were found outside the notch area. The area fraction of the {111} cleavage planes was determined to be approximately 60% of the entire fracture surface. Again approximately 50% of the {111} type cleavage was located near notch area. Therefore, the fracture behavior of the [111] specimen tested in helium can be summarized as fracture mainly on {111} planes in the notch region followed by {111} type cleavage planes outside of the notch area. The cleavage plane orientations near notch and overall area fraction of {111} cleavage planes are given in Table 6.

4. Discussion

The fracture behavior of [100], [110] and [111] single crystals of the PWA 1480E nickel-based superalloy at room temperature has been studied [33]. At room temperature, the crystal with the [100]

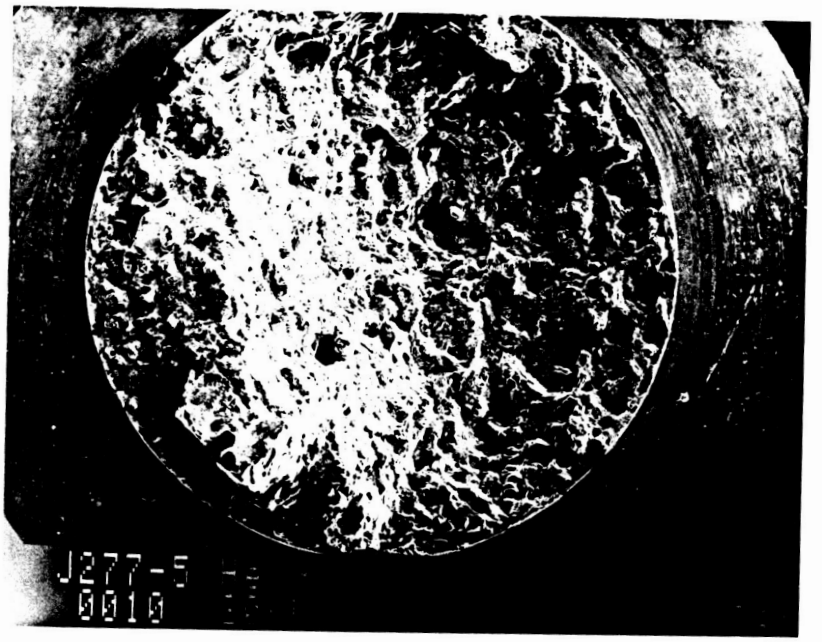

(a)

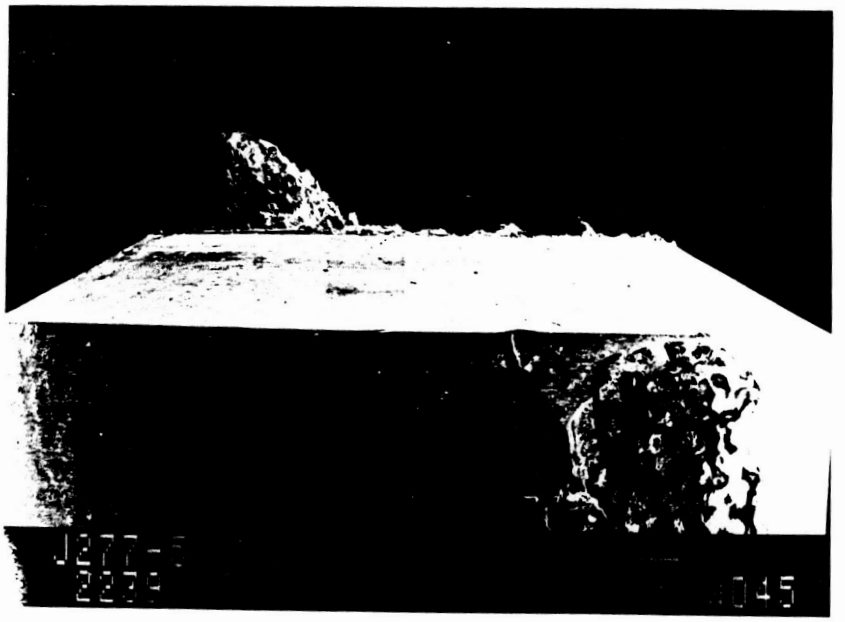

(b)

Figure 15. SEM fractograph of the [110] specimen tested in helium at 871°C; (a) top view. (b) side view.

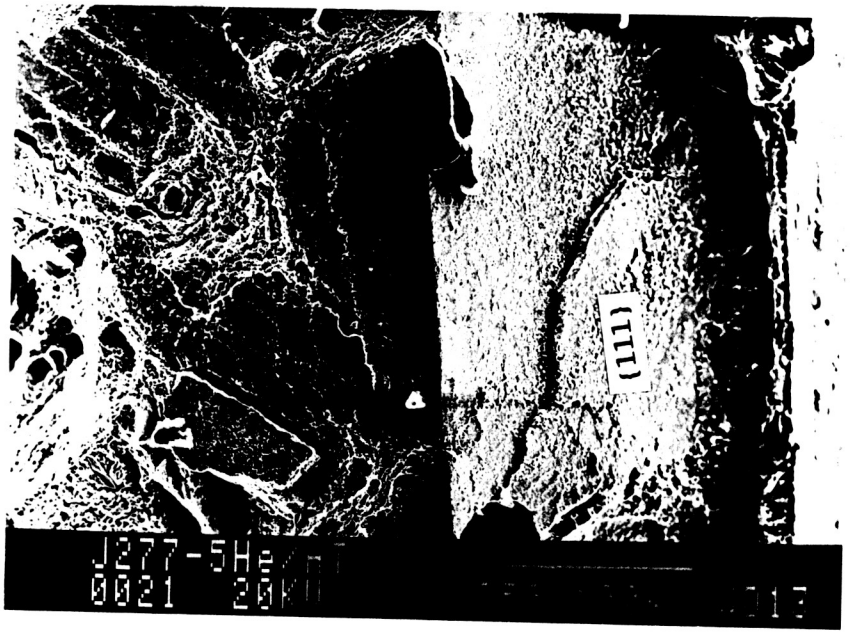

(a)

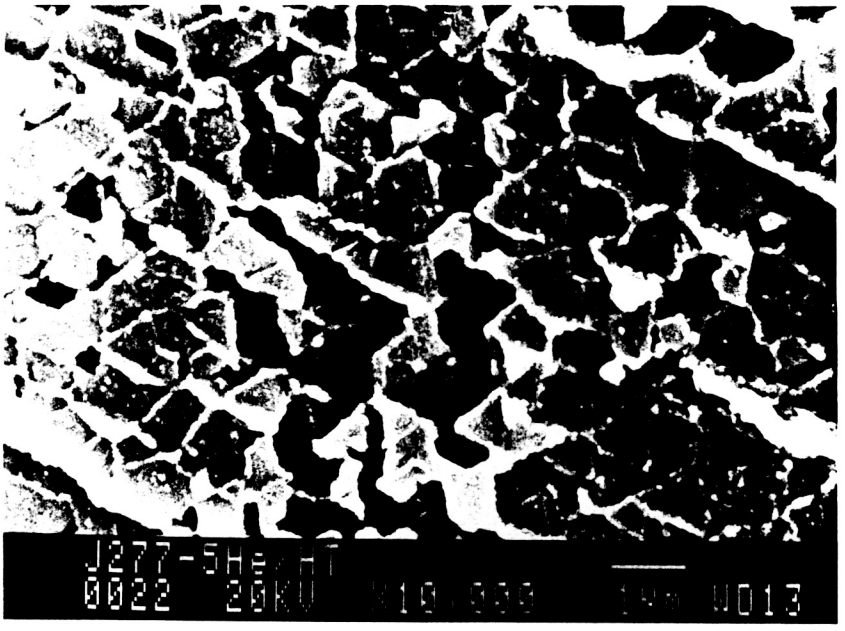

(b)

Figure 16. (a) {111} type of cleavage planes found in the [110] specimen near the notch area. (b) Fractograph taken at high magnification showing a triangular γ network.

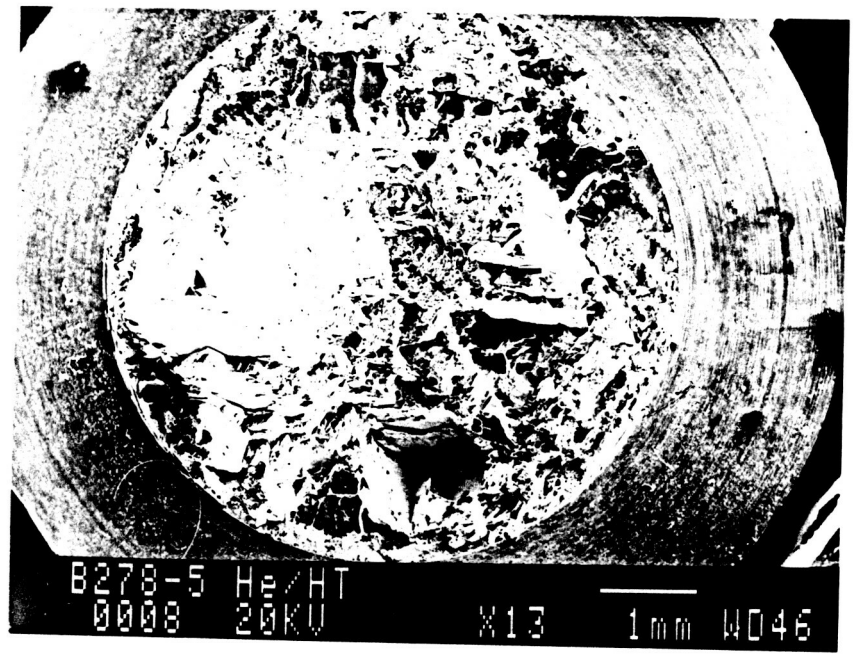

(a)

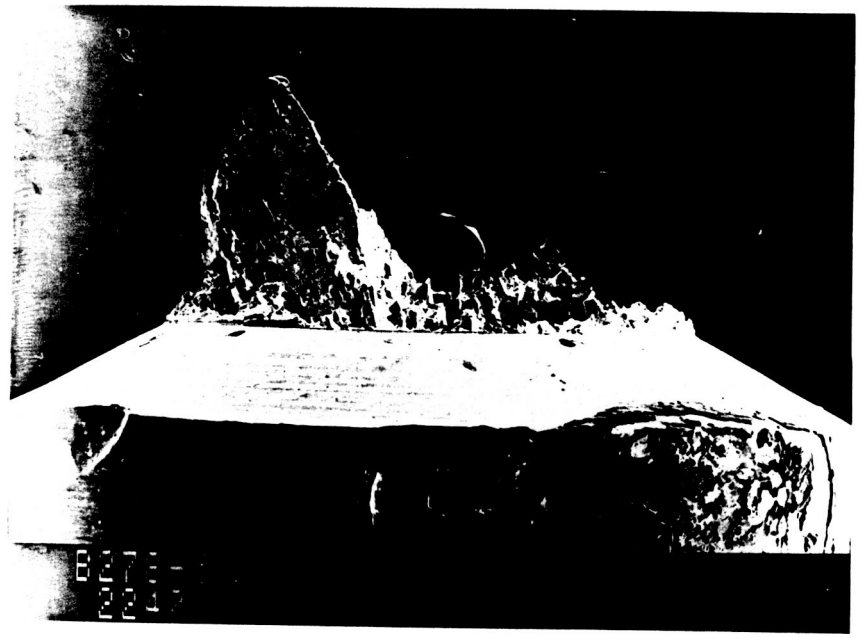

(b)

Figure 17. SEM fractograph of the [111] specimen tested in helium at 871°C; (a) top view. (b) side view.

(a)

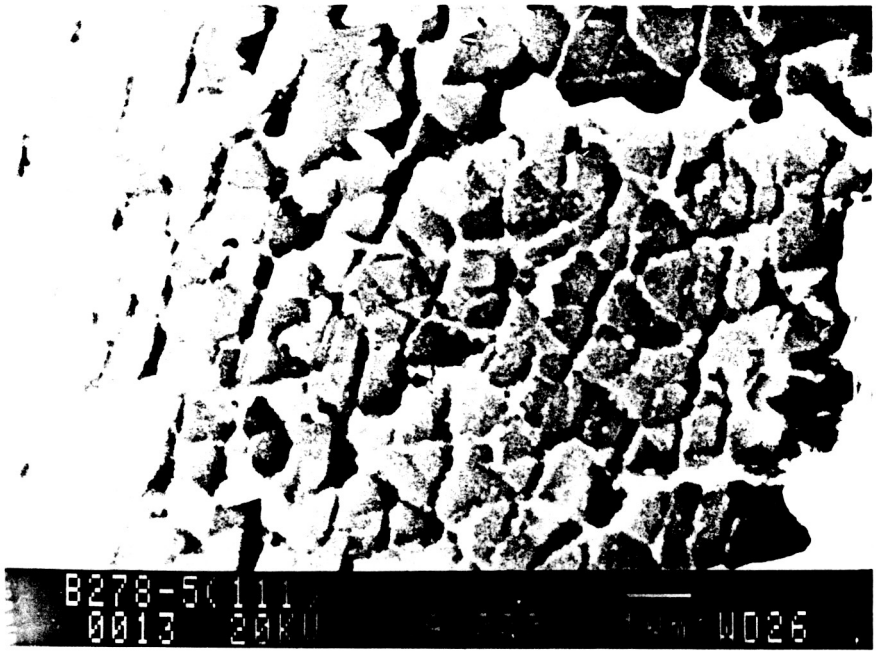

(b)

Figure 18. (a) {111} type of cleavage planes found in the [111] specimen near the notch area. (b) Fractograph taken at high magnification showing a triangular γ' network.

orientation was the weakest while the [110] crystal was the strongest. However, at 871°C the [100] specimen was the strongest of the three crystals while the [110] crystal was the weakest. The [111] specimens exhibited a tensile strength between these two extremes at both room [33] or at high temperature (Table 6). The number of available slip systems along with the γ/γ' interfacial effects were used to interpret the nature of the orientation dependence of the tensile strength.

The orientation and temperature dependence of PWA 1480E single crystals were different compared to the nickel-based alloys, PWA 1480 and Rene N4. Miner et al. [18] have reported that a single crystal of Rene N4 with a [100] orientation exhibited higher tensile strength than a [110] crystal at room temperature, at 760°C or at 980°C. Both [100] and [110] orientations yielded in tension by octahedral slip at all three test temperatures. For the PWA 1480 alloy [18], the [100] orientation was stronger than both the [110] and the [111] orientations in tension for temperatures between 0°C and 980°C. However, at temperatures above 400°C (750°F) the [111] crystal was weaker than both the [100] and the [110] crystals. Shah et al. [19] claimed that all the possible models for deformation including Schmid's factor, Schmid's factor ratio for cube cross slip, and Schmid's factor for the constriction stress all failed to explain this behavior.

In PWA 1480 [18], deformation occurred by octahedral slip near the [100] orientation and by cube-slip near the [111] orientation. In Rene N4 [5], the [100] and [110] crystals yielded by octahedral slip at room temperature, at 760°C and at 980°C, while the specimen with an orientation near [112] deformed by octahedral slip at room temperature

but deformed by cube slip at 760°C and 980°C. A different type of slip behavior was observed in PWA 1480E single crystals tensile tested at room temperature [33]. In these crystals slip on the {111} planes was the controlling factor. In the present study, a similar deformation behavior was observed for the PWA 1480E alloy at 871°C as was observed at room temperature.

Cleavage of all specimens tested in helium occurred primarily on {111} planes despite the single crystal orientation. No obvious macroscopic {100} cleavage was observed on the fracture surface in any of the crystals. In addition, the area fraction of {111} type cleavage planes was found to increase from 25% at room temperature [33] to about 55% at 871°C. This was strong evidence that high temperature promoted {111} octahedral slip and resulted in a large increase in the area fraction of {111} cleavage planes. At room temperature [33], a TEM study showed that deformation occurred along the {111} planes but not by {100} cube slip. Therefore, deformation was assumed to occur primarily by octahedral slip at high temperature because of the large area fraction increasing of {111} cleavage planes and the observed lack of microscopic {100} cleavage.

Dislocations bypassing the γ' particles were not found near the fracture surface at room temperature [33]. On the contrary, dislocations were observed in most areas to accumulate around the γ/γ' interfaces with the γ/γ' interface serving as a strong barrier for dislocation motion. At high temperature, because of the increase in the area fraction of {111} cleavage planes, dislocations seemed to intersect on different {111} slip planes rather than at the γ/γ' interfaces. In

addition, the much rougher (111) cleavage planes in the [100] crystal (Figure 14b), which seemed to occur by pulling of the γ network on (111) cleavage planes, further provided evidence that the γ network suffered plastic deformation during the cleavage propagating process. At 871°C, the dependance of tensile strength on single crystal orientations correlates with the activity of intersecting (111)<110> slip systems. The γ/γ' interface does not act as a strong barrier for dislocation motion at high temperature. Therefore, shearing of γ' particles should control the strength at 871°C.

The deformation behavior of PWA 1480E at 871°C showed good agreement with the No-based alloys Mar-M200 [34] and Rene N4 [18], although a difference was observed with PWA 1480 [18]. In PWA 1480 [18], the [110] crystal had a higher strength than the [111] crystal at temperatures above 450°C. Kear et. al [34] reported that the [110] single crystal oriented for slip on four slip systems exhibited minimum strength at 980°C in Mar-M200. However, the [100] crystal oriented for multiple slip (eight slip systems) had maximum strength. Similar behavior was found in this study.

In PWA 1480E, only four slip systems were available in the [110] crystal so that the possibility of dislocations intersecting from different slip planes was lower compared to the other crystals. The lower the possibility of slip planes intersecting should lead to a decrease in the strength of the [110] specimen. The [100] specimen had highest strength due to the high value of Schmid's factor which led to higher dislocation intersection activity in all eight available slip systems. In the [111] crystals, six slip systems were available and led

to a tensile strength in between the [100] and [110] crystals. Therefore, the strength in PWA 1480E single crystals seemed to be dependent on the number of slip systems available at 871°C but not at room temperature [33]. Interaction of gliding dislocation in different slip systems would be a potential source of work hardening and is believed to be the basis for the different strengths observed.

In PWA 1480E, cleavage planes originated at the notch and propagated along crystallographic planes in all specimens. The observed cleavage planes were either a large single {111} type plane or a combination of smaller {111} planes. The single crystal orientation did not influence the initial cleavage plane orientation in the notch area except for the [110] specimen. In the [110] specimen, $(\bar{1}11)$ and $(1\bar{1}1)$ planes were found outside the notch root but not near the notch area. The absence of $(\bar{1}11)$ and $(1\bar{1}1)$ cleavage planes near the notch region could be because these planes were perpendicular to the [110] tensile axis which resulted in a very small shear stress on these two planes. The presence of $(\bar{1}11)$ and $(1\bar{1}\bar{1})$ outside the notch root could be related to lattice rotation during tensile testing. During the early stage of deformation, lattice rotation could be very small and the Schmid's factor on $(\bar{1}11)$ and $(1\bar{1}\bar{1})$ would be zero. However, after the initial cracks formed near the notch, local lattice rotation could have occurred in the area outside of the notch root and resulted in the Schmid's factor increasing on the $(\bar{1}11)$ and $(1\bar{1}\bar{1})$ planes. The increase in the Schmid's factor on the $(\bar{1}11)$ and $(1\bar{1}\bar{1})$ planes would promote multiple slip on all the {111} planes. The presence of {111} type cleavage planes and fracture ridges outside the notch region should be the result

of simultaneous slip or cross slip on {111} planes [33].

The SEM results of this study suggest the following {111} type cleavage mechanism in helium at 871°C. During the early stage of testing, {111} type slip occurred very quickly in the γ matrix. The γ/γ' interface did not serve as a strong barrier for dislocation motion at high temperature. As loading continued, more intensive planar slip on {111} planes was produced and cut through both the γ matrix and the γ' particles. Once the movements of single {111} slip dislocations were interrupted, cross slip from one {111} to another {111} occurred to keep the dislocations moving. After considerable slip, dislocation entanglements made the movement of dislocations on {111} planes very difficult and resulted in cleavage on {111} crystallographic planes. As the tensile test continued, new mobile dislocations along {111} planes were generated in undeformed areas. These dislocations would not be available for continuing pre-existing {111} slip because most of the dislocations would became sessile near the notch region. When the number of mobile dislocations became too small to provide alternate slip, fracture occurred locally.

B. Fracture in Hydrogen at 871°C

1. [100] Specimen

The top and side view fractographs of the [100] orientated crystal fractured in an hydrogen atmosphere are shown in Figure 19. A jagged appearance which seemed to be the result of cleavage along crystallographic planes in the region of the notch root was found (Figure 20a). Stereoscopic measurements of the normals to the cleavage

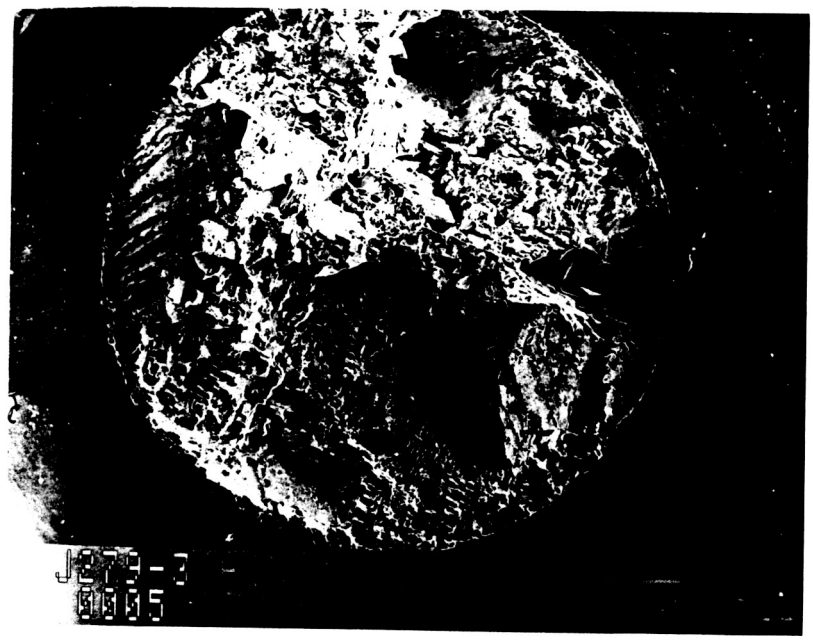

(a)

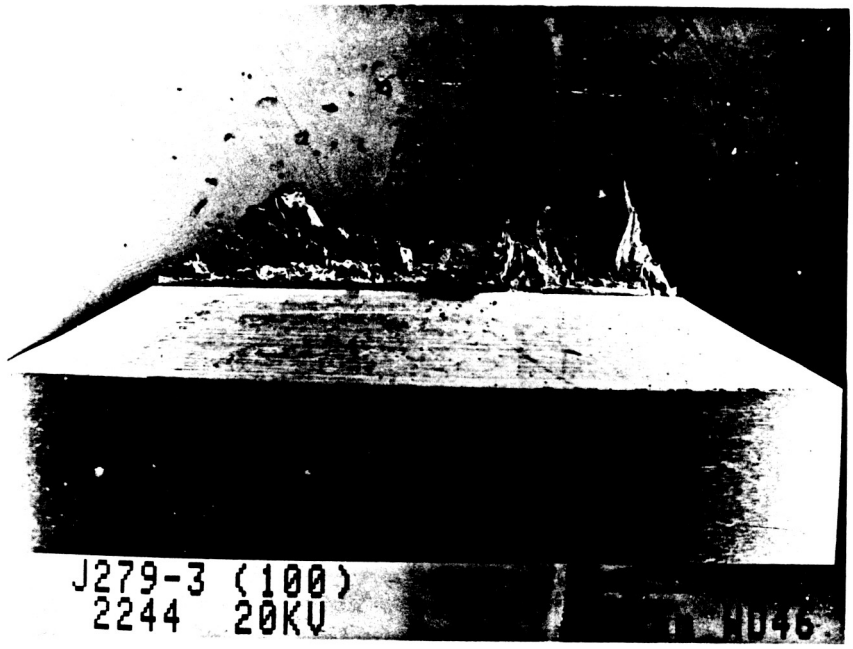

(b)

Figure 19. SEM fractograph of the [100] specimen tested in hydrogen at 871°C; (a) top view. (b) side view.

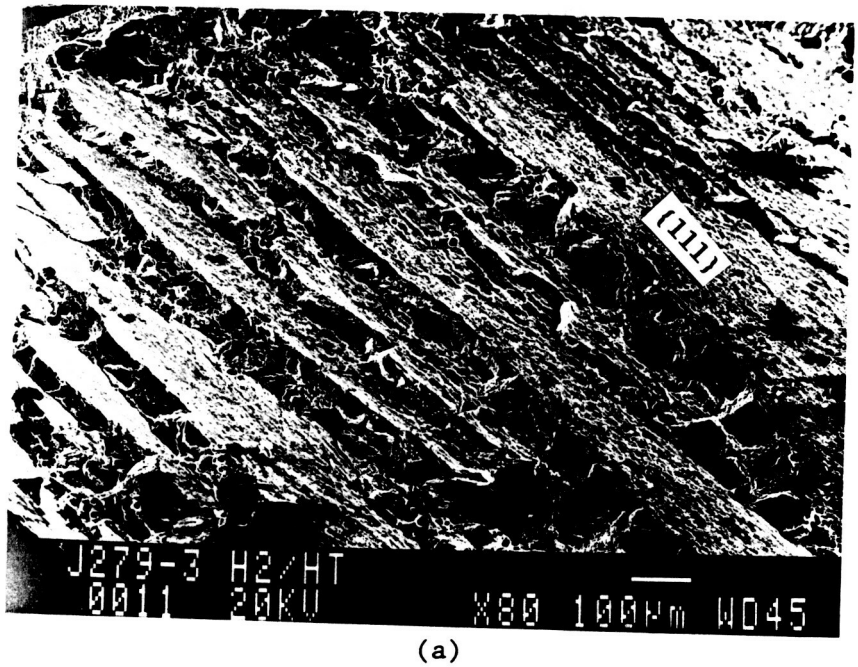

(a)

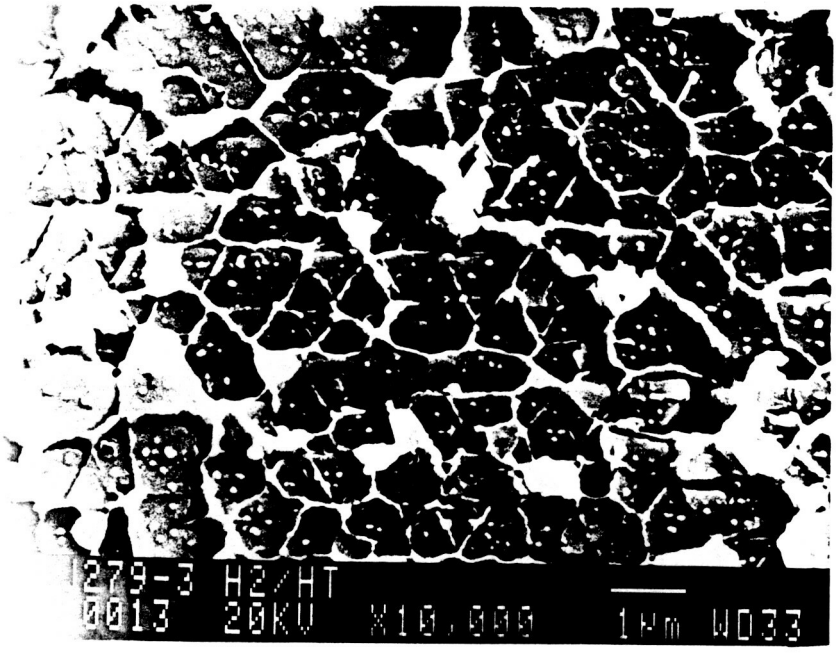

(b)

Figure 20. (a) {111} type of cleavage planes found in the [100] specimen near the notch area. (b) Fractograph taken at high magnification showing a triangular γ' network.

planes near the notch gave an angle of about 55° with respect to the [100] crystal axis. Cleavage planes with this angular relationship were then determined to be {111} type planes. Further examination was made by an equilateral triangular type γ' network (Figure 20b). In addition to the {111} cleavage plane, cleavage on the (100) planes with a square γ' morphology was also detected near the notch root. The (100) cleavage plane was not as smooth as those found in the previous study [10]. The much rougher (100) plane implied that an appreciable amount of plastic deformation occurred before final fracture (Figure 21).

Cleavage on the (100) plane was only found very close to the notch root, however, cleavage on {111} planes was not confined to the notch area. Outside the notch region toward the specimen center, {111} type cleavage planes were detected and further confirmed from the triangular morphology of the γ'. The overall area fraction of {111} type cleavage planes was determined by image analysis to be about 42% of the entire fracture surface. Approximately 50% of the {111} cleavage was located near the notch area. Therefore, the fracture behavior of the [100] specimen tested in hydrogen may be summarized as fracture mainly on the {111} planes in the notch region followed by {111} type cleavage outside of the notch area. The cleavage plane orientations near notch and overall area fraction of {111} cleavage planes are given in Table 7.

2. [110] Specimen

The top and side view fractographs of the [110] specimen are shown in Figure 22. Close examination of the fracture surface revealed several crystallographic cleavage planes. Stereoscopic measurements

gave an angle of 54° between the cleavage plane normals and the [110] crystal axis. These cleavage planes were then determined to be either (111) or ($11\bar{1}$) planes (Figure 23a) and were further confirmed by the appearance of the equilateral triangular type of γ' network (Figure 23b). In addition to the (111) and ($11\bar{1}$) planes found near the notch, {111} cleavage planes were detected outside the notch region toward the specimen center.

The area fraction of the (111) and ($11\bar{1}$) cleavage planes were determined by image analysis to be close to 45%. Approximately 50% of the {111} type cleavage planes were located near the notch area. Therefore, the fracture behavior of the [110] specimen can be summarized as fracture mainly on the (111) and ($11\bar{1}$) type planes in the notch region followed by {111} type cleavage outside the notch area. The cleavage plane orientations near the notch and overall area fraction of {111} cleavage planes are given in Table 7.

3. [111] Specimen

The side view fractograph of the [111] specimen is shown in Figure 24. Closer examination of the fracture surface revealed several crystallographic cleavage planes. Stereoscopic measurements gave an angle of about 70° between the cleavage plane normal and the [111] crystal axis. These cleavage planes were then determined to be of the {111} type planes (Figure 25a). This was further confirmed by the appearance of the triangular type γ' network observed on the cleavage planes (Figure 25b). Therefore, the [111] specimen failed primarily by {111} type cleavage near the notch.

Figure 21. (100) cleavage planes found near the notch root of the [100] crystal showing a square γ' network.

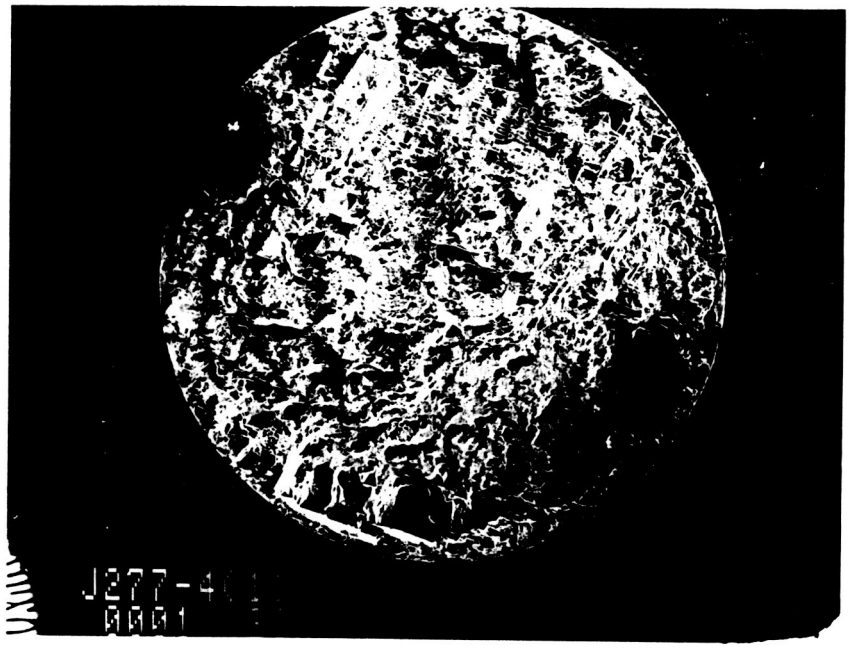

(a)

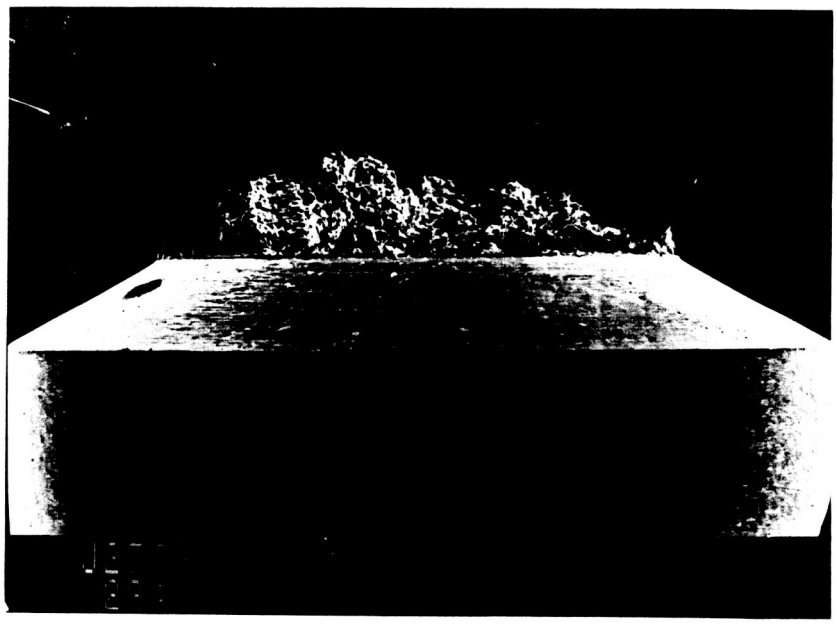

(b)

Figure 22. SEM fractograph of the [110] specimen tested in hydrogen at 871°C; (a) top view. (b) side view.

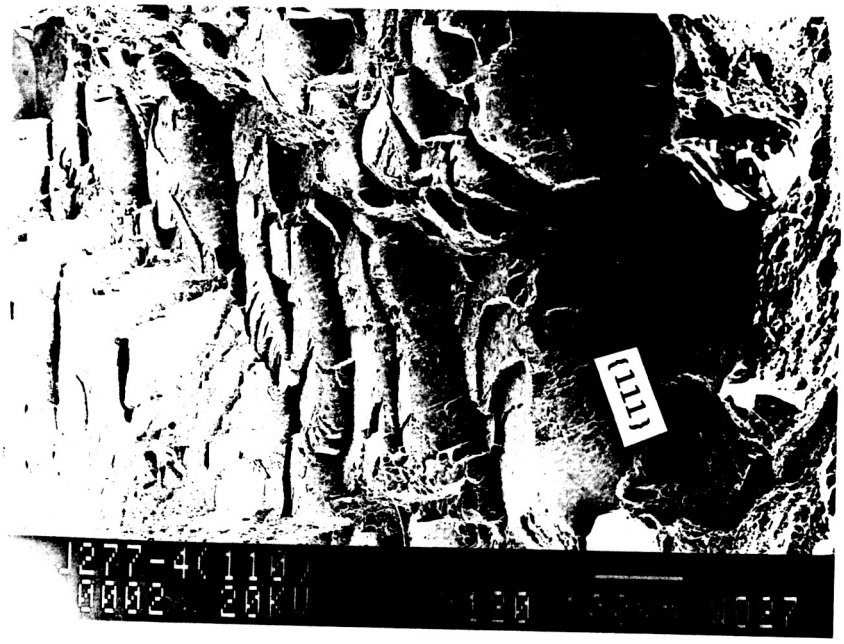

(a)

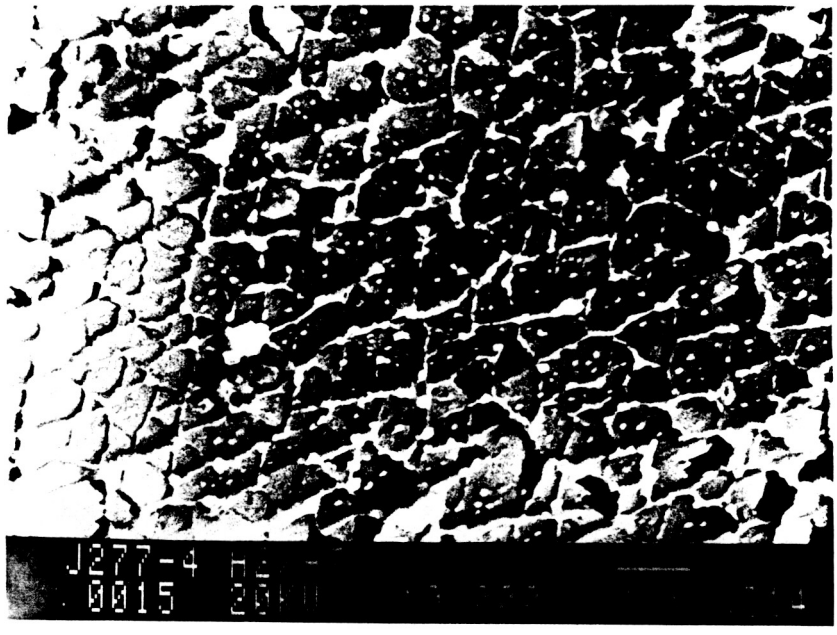

(b)

Figure 23. (a) {111} type of cleavage planes found in the [110] specimen near the notch area. (b) Fractograph taken at high magnification showing a triangular γ' network.

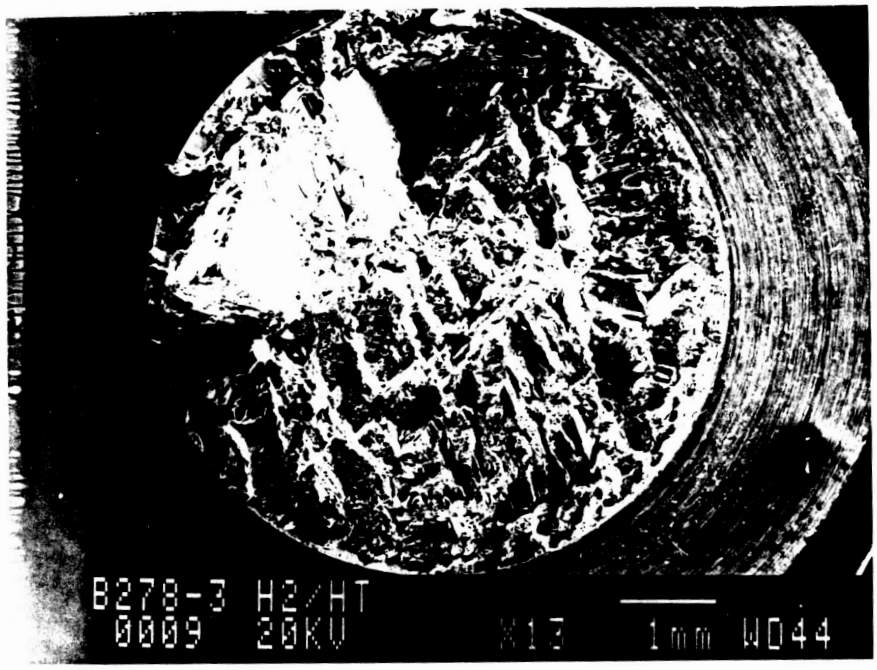

(a)

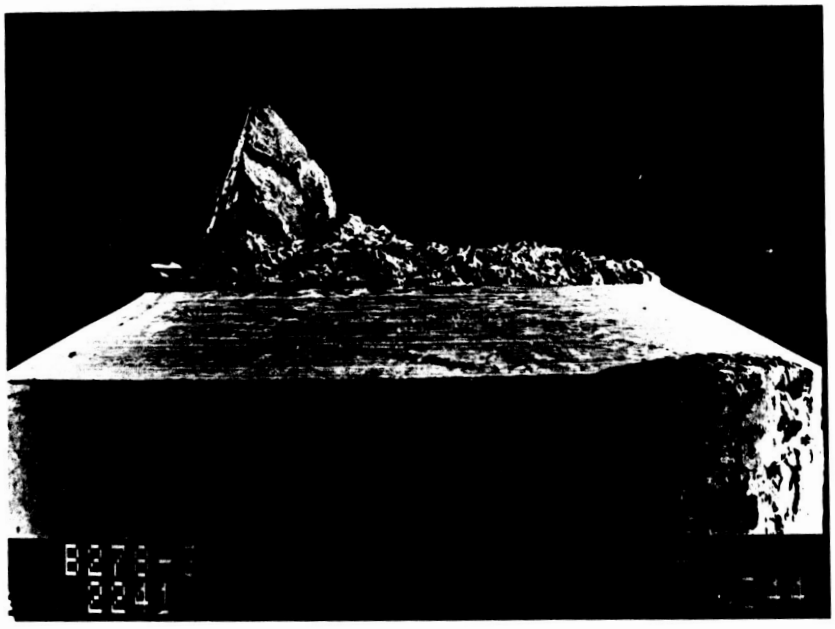

(b)

Figure 24. SEM fractograph of the [111] specimen tested in hydrogen at 871°C; (a) top view. (b) side view.

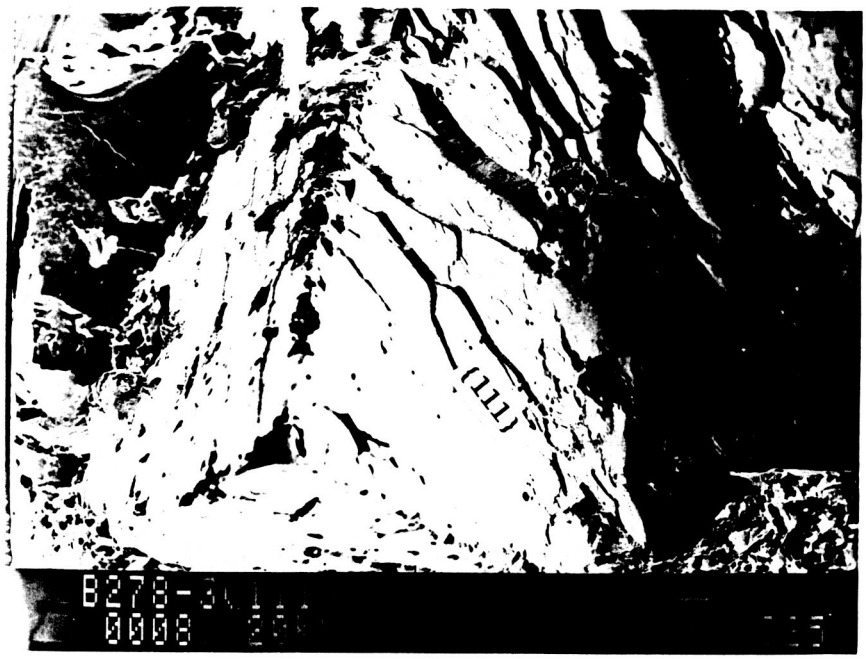

(a)

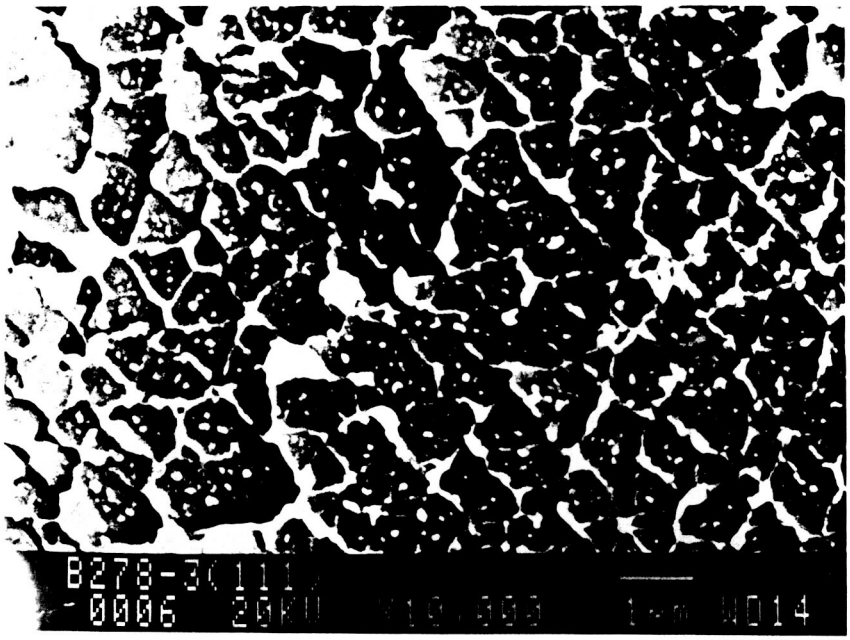

(b)

Figure 25. (a) {111} type of cleavage planes found in the [111] specimen near the notch area. (b) Fractograph taken at high magnification showing a triangular γ' network.

Cleavage planes of the {111} type also were found outside the notch area. The area fraction of the {111} cleavage planes was determined to be approximately 38% of the entire fracture surface. Again approximately 50% of the {111} type cleavage was located near the notch area. Therefore, the fracture behavior of the [111] specimen can be summarized as fracture mainly on {111} planes in the notch region followed by {111} type cleavage planes outside of the notch area. The cleavage plane orientations near the notch and overall area fraction of {111} cleavage planes are given in Table 7.

4. Discussion

The hydrogen-induced fracture behavior of single crystals of the PWA 1480E No-based alloy at room temperature has been studied [33]. At room temperature, the specimen with the [100] orientation was the weakest while the [110] crystal was the strongest. At 871°C, the [111] specimen was the strongest while the [110] crystal was the weakest. The [100] specimen exhibited a tensile strength between these two extremes at high temperature. However, the greatest strength degradation occurred in the [100] specimen but not the [110] crystal as shown in Table 7. The number of available slip systems and γ/γ' interfacial effects were used to interpreted the orientation dependence of the tensile strength at 871°C.

Examination of all the hydrogen charged specimens revealed that fracture occurred predominantly along {111} type of planes near the notch region. The occurrence of {111} cleavage planes in hydrogen charged specimens appeared to be independent of the single crystal

orientation. Hydrogen embrittlement of PWA 1480E alloy at room temperature [33] was found to occur by a highly localized rupture mechanism along the {100} γ/γ' interfaces. For single crystals tested at high temperature, a different fracture behavior was observed. Decohesion along {100} planes was rarely found in the crystals tested at high temperature except for the hydrogen tested [100] specimen. The decohesion of (100) γ/γ' interfaces was found only in some locations near the notch root in the [100] specimen. Also, the (100) cleavage planes were not as smooth as those found at room temperature [33]. Tearing of both γ and γ' phases was observed as shown in Figure 21 and was evidence that hydrogen effects were minimized at high testing temperature. In other words, dislocation accumulation around γ/γ' interfaces as a result of hydrogen effects did not play an important part at high temperature although (100) cleavage still existed in the [100] crystal. Therefore, the γ/γ' interface did not act as a strong barrier to block dislocation motion at high temperature.

Increasing temperature also increased the area fraction of {111} cleavage planes as compared to room temperature [33]. For crystals tested at elevated temperatures, materials properties such as elastic modulus, yield stress change, and environmental interactions become more important [34]. When cross-slip and climb processes become easier at high temperature, deformation becomes more homogeneous. Therefore, the more homogeneous slip at high temperature should change the fracture surface appearance and increase the area fraction of {111} cleavage planes. From these qualitative findings, no significant amount of dislocations were assumed to be trapped along γ/γ' interfaces during

tensile testing at high temperature. Dislocations may be accumulated around γ/γ' interfacial areas during the early stage of deformation, but thermally activated climb and cross-slip could promote dislocation motion without further entanglement. Slip on various {111} planes would finally cause dislocation intersection and then would result in brittle cleavage along {111} planes.

Unlike the large strength difference which occurred at room temperature [33], all specimens tested in hydrogen at 871°C (1600°F) were very close in tensile strength (Table 7). This implied that the effects of hydrogen on orientation differences at high temperature were much less compared to those at room temperature. Therefore, the lower differences in strength must be related to different fracture modes. At room temperature, {100} type cleavage dominated in the three different orientations [33]. However, {111} type cleavage was the controlling fracture mechanism at high temperature. In other words, all crystals tested at high temperature failed primarily by {111} type cleavage regardless the single crystal orientation.

Although the influence of hydrogen was small, hydrogen effects still existed. The most obvious difference was the area fraction of the {111} cleavage planes observed between the two testing atmospheres. For the helium tested crystals, the area fraction of {111} cleavage planes ranged from 50 to 60 %, while only about 38 to 45% of the fracture surface in the hydrogen charged crystals were {111} type cleavage planes. In addition, cleavage along the (100) γ/γ' interface was observed only in very limited areas and the cleavage planes were not as smooth as those found at room temperature [33]. At room temperature,

only about 8 to 10% of the fracture surface was {111} type cleavage planes. This was again evidence that the high temperature environment reduced hydrogen-induced embrittlement along the (100) γ/γ' interface and enhanced slip on {111} planes.

In addition, if {111} type cleavage was the only controlling factor of hydrogen induced fracture, then the [110] specimen would have had the lowest strength just as the one tested in the helium atmosphere did. However, PWA 1480E single crystal with [112] orientation, instead of [110], was reported to have the lowest strength tested in hydrogen atmosphere at 871 °C. Moreover, the [100] crystal had the highest degradation from the crystals tested at room temperature [33]. This was another indication that γ/γ' interfacial decohesion was responsible for a portion of the strength degradation at high temperatures. This further supported the idea that the fracture mechanisms of single crystals tested in hydrogen was the combination of {111} type cleavage and γ/γ' interfacial decohesion. The γ/γ' interfacial decohesion should exist in all the three crystals but was too small to resolve in both the [110] and the [111] crystals. Therefore, the hydrogen embrittlement mechanism at high temperature was more complicated than at room temperature and really was a combination of {111} and {100} type cleavage. Strength degradation would depend on the competition between {111} cleavage and {100} interfacial cracking. The greater the amount of {100} interfacial decohesion, the higher the degradation of strength.

As shown in the previous study [33], the cleavage fracture of hydrogen charged nickel-based superalloy PWA 1480E was mainly governed by {100} cleavage at room temperature. The controlling factor of

anisotropic strength degradation was the small angle between the {100} plane normal and the tensile axis at room temperature. However, the anisotropic degradation of strength in hydrogen charged PWA 1480E single crystals at high temperature could not be explained as a function of the smallest angle between the crystal (tensile) axis and the normal to the {100} planes. This further supported the observation that at 871°C (871°C), {100} cleavage was only responsible for part of the strength degradation but was not the major factor. In other words, hydrogen effects were much reduced at high temperature.

The tensile strength degradation observed in the three crystals [100], [110], and [111] could be explained as follows. Hydrogen enhanced dislocation accumulation near γ/γ' interfacial areas and strengthened the interface. For the [110] specimen, only four slip systems were available. However, the γ/γ' interface provided additional intersecting barriers and resulted in an increase in strength in hydrogen compared to the strength in helium. The [100] specimen had the highest strength in helium, but showed the greatest degradation in hydrogen. This was the result of eight available slip systems which provided more dislocation intersecting possibilities than the other two crystals. However, the largest resolved normal stress on at the (100) γ/γ' interface led to the highest strength degradation.

A possible mechanism of hydrogen induced fracture can be proposed as follows. SEM observations revealed that {111} cleavage was the main controlling factor of hydrogen embrittlement in single crystals of PWA 1480E. At the early stage of tensile testing, {111} slip likely occurred and soon dislocations were trapped in the γ region. Tensile

testing produced planar slip which enhanced dislocation transport and led to high local concentrations of hydrogen in the γ region. The high concentration of hydrogen resulted in severe dislocation pinning and subsequently dislocation accumulation along γ/γ' interfaces and in the γ matrix. The accumulation of dislocation hindered subsequent superdislocation movement. However, at high temperature, thermally activated climb and cross-slip could promote dislocation motion to avoid further entanglement. In the areas with severe entanglement before climb and cross-slip occurred, {100} γ/γ' interfacial decohesion occurred. In other areas, slip on {111} planes continued until slip plane intersections occurred. As tensile testing continued, new mobile dislocations along {111} planes were generated in the undeformed area. When mobile dislocations became exhausted, cleavage was accelerated and finally fracture occurred.

The following summaries resulted from this investigation of hydrogen-induced fracture in single crystals of the nickel-based superalloy PWA 1480E at 871°C:

1. Tensile induced primary {111} cleavage in both hydrogen and helium likely originated from combined slip on {111} planes.
2. The availability and activity of slip systems appeared play an important part in the strength variation between different orientations in helium.
3. Hydrogen promotes γ/γ' interfacial decohesion although macroscopic (100) cleavage was only observed in the [100] specimen.
4. Cracking on the (100) plane, likely along the γ/γ' interface

affects the strength in hydrogen although only very limited (100) cleavage plane was observed in the specimens tested in hydrogen.

5. The strength variation in hydrogen charged specimens depends on the combination of (100) cleavage and {111} slip.
6. The strength increasing in the [110] crystal in hydrogen is very likely due to γ/γ' interfacial dislocation accumulation which provides extra strengthening effects.
7. The largest resolved normal stress on (100)plane led to highest strength degradation in the [100] crystal.
8. The occurrence of {111} type of cleavage was qualitatively independent of the single crystal orientations and testing atmosphere.
9. The specimens tested in helium revealed more area fraction of {111} cleavage planes than hydrogen.

V. CONCLUSIONS

The following conclusions resulted from the investigation of hydrogen induced fracture in notched single crystals of the nickel-based superalloy PWA 1480E. These also include the conclusions from the Final Report dated July 15, 1989 [15].

1. The lattice mismatch, misorientation, volume fraction of γ' in PWA 1480 Nickel-base superalloy were independent of single crystal orientation.

2. γ' particles are orderly and closely aligned with edges along the [100], [010] and [001] directions. Different crystal growth orientations did not affect the morphology of γ' particles.

3. Tensile induced {111} cleavage in helium originated from combined slip on {111} planes. The occurrence of {111} type of cleavage was qualitatively independent of the single crystal growth orientations.

4. Dislocation accumulation around the γ/γ' interface forming strong barriers for subsequent dislocation movement, is the primary strengthening mechanism at room temperature.

5. The availability and activity of slip systems played an important part to the strength variation between different orientations.

6. Cracking along γ/γ' interface was not observed in all the helium-charged specimens with seven different crystal growth orientations.

7. Hydrogen enhanced cleavage along {100} planes was the most important mechanism of hydrogen-induced embrittlement in single crystals of PWA 1480E.

8. {100} type cleavage in hydrogen was associated with either cracking along the γ/γ' interfaces or along {111} planes in the γ matrix. The occurrence of {100} type of cleavage was qualitatively independent of the single crystal orientations.

9. The angle between the normal to the {100} planes and the crystal orientation had a strong influence on the strength degradation at room temperature.

10. The absence of {100} type planes in the helium charged specimens supported that {100} cleavage was induced by hydrogen at room temperature.

11. Tensile induced primary {111} cleavage in both hydrogen and helium originated from combined slip on {111} planes at 871°C.

12. The availability and activity of slip systems played an important part to the strength variation between different orientations in helium at high temperature.

13. The strength variation in a hydrogen charged specimen likely depended on the combination of γ/γ' interfacial dislocation accumulation and {111} slip.

14. The strength increase in the [110] crystal in hydrogen was likely due to the γ/γ' interfacial dislocation accumulation which provided extra strengthening effects.

15. The largest resolved normal stress on the (100) γ/γ' interface led to the highest strength degradation in the [100] crystal.

16. The occurrence of {111} type of cleavage was qualitatively independent of the single crystal orientations and testing atmosphere at 871°C.

VI. REFERENCES

1. R.L. Dreshfield and R.A. Parr, "Application of Single Crystal Superalloys for Earth-to Orbit Propulsion System," **NASA Memorandum** 89877, ALAA-87-1976.

2. B.H. Rear, "Advanced Metals," **Scientific American**, pp. 159-167 (October 1986).

3. M.V. Nathal and L.J. Ebert, "The Influence of Cobalt, Tantalum, and Tungsten on the Microstructure of Single Crystal Nickel-Base Superalloys," **Met. trans.**, Vol. 16A, pp. 1859-1862 (October 1985).

4. R.V. Miner, T.P. Gabb, J. Gayda and K.J. Hemker, "Orientation and Temperature Dependence of Some Mechanical Properties of the Single-Crystal Nickel-Base Superalloy Rene N4: Part III. Tension-Compression Anisotropy," **Met. Trans.**, Vol. 17A, pp. 507-512 (March 1986).

5. R.V. Miner, R.C. Voigt, J. Gayda, and T.P. Gabb, "Orientation and Temperature Dependence of Some Mechanical Properties of the Single-Crystal Nickel-Base Superalloy Rene N4: Part I. Tensile Behavior," **Met. Trans.**, Vol. 17A, pp. 491-496 (March 1986).

6. M. Dollar and I.M. Bernstein, "The Effect of Hydrogen on Deformation Substructure, Flow and Fracture in a Nickel-Base Crystal Superalloy," **Acta Metall.**, Vol. 36, No. 8, pp. 2369-2376 (1988).

7. C.L. Baker, J. Chene, I.M. Bernstein and J.C. Williams, "Hydrogen Effects in [001] Oriented Nickel-Base Superalloy Single Crystals," **Met. Trans.**, Vol. 19A, pp. 73-82 (January 1988).

8. N.F. Foire and J.A. Kargol, "Hydrogen-Related Embrittlement of Ni-Base Superalloy," **Hydrogen Effects in Metal: Proceedings of the 3rd International Conference on Effects of Hydrogen on Behavior of Metals**, I.M. Bernstien and A.W. Thompson, Eds., Metallurgical Society of AIME, Warrendale, PA., pp. 851-862.

9. H. Vehoff and H.K. Klameth, "Hydrogen Embrittlement and Trapping at Crack Tips in Ni-Single Crystals," **Acta Metall.**, Vol.33, No. 6, pp. 955-962 (1985).

10. I.M. Robertson and H.K. Birnbaum, "An HVEM Study of Hydrogen Effects on the Deformation and Fracture of Nickel," **Acta Metall.**, Vol. 34, No. 3, pp. 353-366 (1986).

11. S. Hinttani, Y. Ohmori and F. Terasaki, "Effect of Nickel Hydride Formation and Hydrogen Embrittlement in Ni-Cr-Fe Alloys," **Materials Science and Engineering**, Vol. 74, pp. 119-131 (1985).

12. E. Lunaraka-Borowiecka and N.F. Fire, "Hydride Formation in a Ni-Base Superalloy," **Met. Trans.** Vol. 12A, pp. 101-107 (1981).

13. S. Hinotani, Y. Ohmori and F. Terasaki, "Effects of Phosphorus Segregation and Ni_2Cr Formation on Hydrogen Embrittlement in 70Ni-30Cr Alloys," **Materials Science and Technology**, Vol. 1, pp. 197-304 (April 1985).

14. N.F. Foire and J.A. Kargol, "Hydrogen-Related Embrittlement of Ni-Base Superalloy," **Hydrogen Effects in Metal**, pp. 851-862.

15. P. S Chen and R. C. Wilcox, "Hydrogen Induced Fracture Characteristic of Single Crystal Nickel-Based Superalloy," **NASA Final Report**, NAS8-36654 (1989).

16. O.H. Kriege and C.P. Sullivan, "The Separation of Gamma Prime from Udimet 700," **Transactions of the ASM**, Vol. 61 pp. 278-282 (1968).

17. J.M. Obloak and B.H. Kear, "Characterization of Coherent Ordered Precipitates in Nickel-Base alloys," **Physical Aspects of Electron Microscopy and Analysis**, (Ed. Siegel Beaman), pp. 149-162, Wiley, New york (1975).

18. D.M.Shah and D.N.Duhl,"The Effect of Orientation, Temperature and Gamma Prime Size on the Yield Strength of a Single Crystal Nickel Base Superalloy," **Superalloys 1984**, M. Gell, C.S.Kortovich, R.H.Bricknell, W.B.Kent, and J.F.Radavich, eds., AIME, Warrendale, PA, 1984, pp. 105-114.

19. D.L. Anton, "Fracture of Nickel-Base Superalloy Single Crystals," **Materials Science and Engineering**, Vol. 57,pp. 97-105 (1983).

20. K. Aoki and O. Izumi, "Cleavage Fracture of the Intermetallic Compound Ni_3Ge Single Crystal," **Acta Metall.**, Vol. 27, pp. 807 -816 (1979).

21. A.A. Hopgood and J.W. Martin, "The Effect of Aging on the Yield Stress of a Single-Crystal Superalloy," **Materials Science and Engineering**, Vol. 91, pp. 105-110 (1987).

22. D.R. Muzyka, "Physical Metallurgical and Effects of Process Variables on the Microstructure of Wrought Superalloys," **Superalloy Source Book**, pp. 248-268, ASM, Metals Park, Ohio (1984).

23. P. Caron and T.Khan, "Improvement of Creep Strength in a Nickel-Base Single-Crystal Superalloy by the Heat Treatment," **Materials Science and Engineering**, Vol. 61, pp. 173-184 (1983).

24. K.S. Chan, J.E. Hack and G.R. Leverant, "Fatigue Crack Growth in Mar-M200 Single Crystals," **Met. Trans.**, Vol. 18A, pp. 581-591 (April 1987).

25. M.V. Nathal and L.J. Ebert, "Elevated Temperature Creep-Rupture Behavior of the Single Crystal Nickel-Base Superalloy," **Met. Trans.**, Vol. 16A, pp. 427-439 (March 1985).

26. G.N. Maniar and J.E. Bridge, "Effect of Gamma-Gamma Prime Mismatch, Volume Fraction Gamma Prime, and Gamma Prime Morphology on Elevated Temperature Properties of Ni, 20Cr, 5.5Mo, Ti, Al Alloys," **Met. Trans.**, Vol. 2A, pp. 95-102 (1971).

27. K.S. Chan, J.E. Hack and G.R. Leverant, "Fatigue Crack Growth in Mar-M200 Single Crystals under Multiaxial Cyclic Loads," **Met. Trans.**, Vol. 17A, pp. 1739-1750 (October 1986).

28. G.E. Dieter, **Mechanical Metallurgy**, McGraw-Hill Book Company, New York (1986).

29. A. Huis in't Veld, G. Boom, P. M. Bronsveld, J. Th. M. De Hosson, "Superlattice Dislocations on {111} and {001} in Superalloy," **Scripta Metall.**, Vol. 19, pp. 105-110 (1985).

30. M.V. Nathal, "Effect of Initial Gamma Prime Size on the Elevated Temperature Creep Properties of Single Crystal Nickel Base Superalloy," **Met. Trans.**, Vol. 18A, pp. 1961-1970 (November 1987).

31. R.V. Miner, J. Gayda and R.D. Maier, "Fatigue and Creep-Fatigue Deformation of Several Nickel-Base Superalloys at 650°C," **Metall. Trans.**, Vol. 13A, pp. 1755-1765 (1982).

32. J. Pielaszek, "Hydrogen Embrittlement," **Hydrogen in Metals**, G. Alefeld and J. Volkl, Eds., Springer-Verlag, New York, NY, (1978) pp.105-128.

33. P.S.Chen, R.C.Wilcox, "Hydrogen Induced Cleavage in Single Crystals of the Ni-based Superalloy PWA 1480E," **International Metallographic Society**, 22nd Annual Convention, Charlotte, N.C., July 25-26, 1989.

34. B. H. Kear and B. J. Piearcey, " Tensile and Creep Properties of Single Crystals of The Nickel-Base Superalloy Mar-M200," **Trans. AIME**, Vol. 239, pp. 1209-1215 (1967).